### Title
Distinct regional and subcellular localization of the actin-binding protein filamin A in the mature rat brain.




### Journal
The Journal of comparative neurology, 520(13)

### ISSN
0021-9967



### Authors
Noam, Yoav
Phan, Lise
McClelland, Shawn
et al.



### Publication Date
2012-09-01

### DOI
10.1002/cne.23106

Published in final edited form as:
*J Comp Neurol*. 2012 September 1; 520(13): 3013–3034. doi:10.1002/cne.23106.

# Distinct Regional and Subcellular Localization of the Actin-Binding Protein Filamin A in the Mature Rat Brain

**Yoav Noam**[1,2], **Lise Phan**[1], **Shawn McClelland**[1], **Erik M. Manders**[3], **Markus U. Ehrengruber**[1], **Wytse J. Wadman**[2], **Tallie Z. Baram**[1], and **Yuncai Chen**[1,*]

[1]Departments of Anatomy/Neurobiology and Pediatrics, University of California—Irvine, Irvine, California 92697-4475 [2]SILS-Center for Neuroscience, University of Amsterdam, 1098XH Amsterdam, The Netherlands [3]Center for Advanced Microscopy (CAM), University of Amsterdam, 1098XH Amsterdam, The Netherlands

## Abstract

Filamin A (FLNa) is an actin-binding protein that regulates cell motility, adhesion, and elasticity by cross-linking filamentous actin. Additional roles of FLNa include regulation of protein trafficking and surface expression. Although the functions of FLNa during brain development are well studied, little is known on its expression, distribution, and function in the adult brain. Here we characterize in detail the neuroanatomical distribution and subcellular localization of FLNa in the mature rat brain, by using two antisera directed against epitopes at either the N′ or the C′ terminus of the protein, further validated by mRNA expression. FLNa was widely and selectively expressed throughout the brain, and the intensity of immunoreactivity was region dependent. The most intensely FLNa-labeled neurons were found in discrete neuronal systems, including basal forebrain structures, anterior nuclear group of thalamus, and hypothalamic parvocellular neurons. Pyramidal neurons in neocortex and hippocampus and magnocellular cells in basolateral amygdaloid nucleus were also intensely FLNa immunoreactive, and strong FLNa labeling was evident in the pontine and medullary raphe nuclei and in sensory and spinal trigeminal nuclei. The subcellular localization of FLNa was evaluated *in situ* as well as in primary hippocampal neurons. Punctate expression was found in somata and along the dendritic shaft, but FLNa was not detected in dendritic spines. These subcellular distribution patterns were recapitulated in hippocampal and neocortical pyramidal neurons *in vivo*. The characterization of the expression and subcellular localization of FLNa may provide new clues to the functional roles of this cytoskeletal protein in the adult brain.

### INDEXING TERMS

FLNa; ABP-280; dendrite; immunocytochemistry; rodent

The actin network is composed of highly organized structures that not only determine the morphology of the cell but also influence cellular signaling by controlling trafficking and distribution of membrane-bound proteins. In neurons, the actin network plays crucial roles in neurite differentiation, dendritic branching, spine dynamics, and synaptic transmission (Cingolani and Goda, 2008; Pak et al., 2008). Among the various building blocks that make up the actin scaffold, filamin A (FLNa) is a protein that promotes a three-dimensional,



*CORRESPONDENCE TO: Yuncai Chen, PhD, Med Sci B180, ZOT 4475, University of California—Irvine, Irvine, CA 92697-4475. yuncaic@uci.edu.

orthogonal network organization by cross-linking filamentous actin in a perpendicular orientation (Stossel et al., 2001; Nakamura et al., 2007). These unique cross-linking features endow FLNa with important roles in regulating cellular structure, motility, and elasticity across a variety of tissues and cell types (Popowickz et al., 2006; Nakamura et al., 2011).

In addition to its structural roles, FLNa binds to various ion channels, receptors, and other signaling molecules and thus influences their distribution, trafficking, and function. For example, FLNa facilitates surface expression of the potassium channel subtypes Kir2.1, Kv4.2, and $BK_{Ca}$ (Petrecca et al., 2000; Sampson et al., 2003; E.Y. Kim et al., 2007) and inhibits surface expression and function of the nonselective cationic HCN1 channel (Gravante et al., 2004). Other roles include regulating agonist-induced internalization and G-protein binding of μ opioid receptors (Onoprishvili et al., 2003; Wang et al., 2008) and controlling the functional properties of dopamine D2 receptors and HCN1 channels (Li et al., 2000; Gravante et al., 2004). Accumulating evidence suggests that interaction of FLNa with receptors and ion channels takes place also in the brain: FLNa was found to associate with $G_o$-coupled μ opioid receptors and with Kv4.2 channels in the adult rat striatum and in cerebellum, respectively (Petrecca et al., 2000; Wang et al., 2008), and HCN1 channel protein was coimmunoprecipitated with FLNa in the bovine brain (Gravante et al., 2004). Furthermore, FLNa colocalizes with Kv4.2 channels and D2 receptors in primary neuronal cultures (Petrecca et al., 2000; Lin et al., 2001).

FLNa has been the subject of intense research in the *developing* mammalian brain, in which it serves critical roles in neuronal migration. Loss-of-function mutations in the *FLNa* gene have been strongly associated with human periventricular heterotopia (see, e.g., Fox et al., 1998; Sheen et al., 2005; Parrini et al., 2006). In this disorder, aberrant FLNa hinders migration of neurons either by interfering with actin remodeling or by destabilizing the surface lining and the organization of radial glia in the ventricular zone (Sarkisian et al., 2008; Carabalona et al., 2012). In accordance with its importance for brain development, FLNa is expressed in high levels in the prenatal and neonatal brain, and these levels diminish during adolescence to reach steady, moderate expression in adulthood (Fox et al., 1998; Sheen et al., 2002).

Although the presence of FLNa in the adult brain has been well documented (see, e.g., Fox et al., 1998; Petrecca et al., 2000; Sheen et al., 2002; Wang et al., 2008), a systematic analysis of its expression patterns and subcellular distribution is lacking. Such characterization can be especially helpful in light of the potential roles that FLNa may play in receptor and ion channel trafficking. In this study, we combine immunocytochemical approaches *in vivo* and *in vitro* to characterize the selective expression of FLNa in the rat brain and the subcellular localization of this actin-binding protein in mature neurons.

## MATERIALS AND METHODS

### Animals

Sprague-Dawley rats aged 0, 16, 90, and 120 days were used in this study. Animals were kept on a 12-hour light/dark cycle and given free access to food and water. All experiments were carried out according to NIH guidelines for the care of experimental animals, with approval by the University of California Institutional Animal Care and Use Committee (IACUC).

### Antibody characterization

A list of the antibodies used in this study and their details is provided in Table 1. Further information is pro-vided below.

### FLNa

Two FLNa antibodies, raised against either the C′ or the N′ terminus of the protein, were used in this study. Detailed assessment of their specificity, as determined by Western blot, immunocytochemistry, and *in situ* hybridization, is provided in Results.

### MAP2

A monoclonal anti-microtubule-associated protein 2 (MAP2) antibody was used as a dendritic marker (clone HM-2). The antibody was made by immunizing mice against microtubule-associated protein, which was fractionated from purified rat brain microtubules (Huber and Matus, 1984). Western blot experiments on rat brain homogenates yielded a single band that corresponded to the predicted molecular weight of MAP2, whereas no signal was detected in tissues devoid of MAP2, such as lung, liver, and heart (Huber and Matus, 1984). Immunolabeling of hippocampal neurons resulted in a typical dendritic staining pattern (Lim et al., 2008), which was reproduced in our study (Fig. 11).

### GAD65

A monoclonal glutamic acid decarboxylase 65 (GAD65) antibody was used as an interneuronal marker (Millipore, Bedford, MA; clone GAD6). This antibody was raised against purified rat brain GAD and recognizes the lower molecular weight form of the protein upon Western blotting of unfractionated rat whole brains as well as of purified GAD protein (Chang and Gottlieb, 1988). Although a similar single band was observed in Western blots of mouse brain extracts, it was completely absent in GAD65 knockout mice (Yamamoto et al., 2004). The distribution pattern of GAD65 in rat neurons has been previously described with the same antibody (see, e.g., Rostkowski et al., 2009). Consistently with previous studies, the typical punctate distribution of GAD65 along GABAergic axon terminals and in interneuronal somata was observed in our hands (Fig. 10).

### PSD-95

Postsynaptic density protein 95 (PSD-95) is an established marker for postsynaptic structures, and these are typically found on dendritic spines. The monoclonal antibody used in our study (clone 7E3-1B8) was selected after immunizing mice against recombinant rat PSD-95 (Kornau et al., 1995). The specificity of the antibody has been demonstrated in Western blotting (manufacturer's information sheet and Kornau et al., 1995). A typical, punctate synaptic expression pattern (which is colocalized with other synaptic proteins) has been described in immunolabeling studies using both light and electron microscopy (Kornau et al., 1995; Koulen et al., 1998; Lepousez et al., 2010).

### GluR1

The rabbit anti-GluR1 antibody used here has been extensively characterized in both light and electron microscopic studies (e.g., King et al., 2006; Das et al., 2008). It recognizes a single band that corresponds to the expected molecular weight of GluR1 (Wenthold et al., 1992) and shows no signal in immunoblots from GluR1 knockout animals (Zamanillo et al., 1999).

### Western blot analysis

Sprague-Dawley rats of different ages (P0, P16, P120) were used for protein analysis. Animals were decapitated and the brains were rapidly dissected and placed in prelabeled microcentrifuge tubes residing in a container filled with dry ice and stored at −80°C until homogenization and processing. The tissue was homogenized in glass/Teflon homogenizers in cold RIPA buffer (50 mM Tris-HCl, pH 7.4, 1% NP-40, 1% Triton X-100, 1 mM EDTA,

150 mM NaCl, 1 × PIC). After homogenization, samples were centrifuged at 16,000*g* for 5 minutes at 4°C. Protein concentration was determined using a Bio-Rad Protein assay (Bio-Rad, Hercules, CA).

Protein samples (30 μg) were suspended in Laemmli buffer, separated by 4–12% SDS-PAGE and visualized using an enhanced chemiluminesence ECL-Plus kit (Amersham Pharmacia Biotech, Arlington Heights, IL). After SDS-PAGE, samples were transferred to PVDF membranes (Amersham Pharmacia Biotech), and nonspecific binding was blocked by incubation with 10% nonfat milk in phosphate-buffered saline (PBS) for 1 hour at room temperature. Membranes were probed with anti-FLNa or anti-actin antibodies (Table 1) in PBS with 5% nonfat milk overnight at 4°C, followed by washes in PBS containing 1% Tween (PBS-Tw; 6 × 5 minutes). Membranes were then incubated with horseradish peroxidase (HRP)-conjugated anti-rabbit or -mouse IgG (1:10,000; Amersham Pharmacia Biotech) in PBS for 1 hour at room temperature. After final washes in PBS-Tw (4 × 15 minutes), membranes were incubated with ECL-Plus (GE Healthcare Life Sciences, Little Chalfont, United Kingdom) for 5 minutes, and immunoreactive bands were visualized by apposing membrane to Hyperfilm ECL (GE Helathcare Life Sciences). A series of ECL exposures was carried out to ensure that nonsaturated bands were used for quantification. Western blot data acquisition and analysis were accomplished by measuring the pixel density and area of immunoreactive bands from the ECL films in UTHSCSA ImageTool software. The optical density values of FLNa were subsequently normalized to the values obtained from the actin-immunoreactive (-ir) band.

## Primary neuronal cultures

Dissociated primary neuronal cultures were prepared from hippocampi of postnatal day 0 (P0) rats as previously described (Noam et al., 2010). Briefly, hippocampi were dissected and separated from adherent tissue, followed by 30 minutes of incubation with 10 U/ml of the protease papain (Worthington, Lakewood, NJ). Papain was removed by a series of washes in decreasing concentrations of the papain inhibitor ovomucoid (Sigma-Aldrich, St. Louis, MO). Cells were mechanically triturated and plated at a density of 200–400 cells/$mm^2$ on 12-mm glass coverslips that had been precoated with poly-D-lysine (Sigma-Aldrich). On the third day in culture, 1 μM of the mitotic inhibitor cytosine arabinoside (Sigma-Aldrich) was added in order to limit glial growth. The neuronal cultures were refreshed twice per week with a preconditioned medium that was prepared by incubating confluent non-neuronal cultures prepared from P3–P4 rat cortices with Neurobasal medium and B27 supplement (Invitrogen, Carlsbad, CA) for 24 hours. Cultures were maintained for 3–4 weeks in a humidified incubator, at 36°C and 5% $CO_2$.

## Immunocytochemistry (ICC) of neuronal cultures

Glass coverslips containing 3–4-week-old neuronal cultures were washed briefly with ice-cold 0.01 M PBS solution and fixed in 4% paraformaldehyde for 20 minutes on ice, followed by a series of washes with PBS (5 × 5 minutes). Cells were permeabilized with 0.1% Triton X − 100 in PBS for 10 minutes, followed by 1 hour of incubation with a blocking solution (1% bovine serum albumin [BSA] and 5% goat serum in PBS) at room temperature. Primary antibodies were diluted in PBS containing 1% BSA and were applied overnight at 4°C using the dilutions described in Table 1. On the following day, primary antibodies were removed by a series of washes, and a secondary antibody, Alexa Fluor 488/568 goat anti-rabbit or anti-mouse IgG (1:400; Invitrogen), was applied for 30 minutes at room temperature, protected from light. After the removal of the secondary antibody, coverslips were washed three times with PBS at 5-minute intervals and mounted on a coverglass using Fluoromount G mounting gel (Southern Biotechnology, Birmingham, AL).

### Tissue preparation, immunocytochemistry of brain slices, and semiquantitative analysis

P90 male rats (n = 4) were perfused via the ascending aorta with 0.9% saline solution followed by perfusion with 4% paraformaldehyde solution made in 0.1 M PB (pH 7.4, 4°C). Brains were postfixed for 3 hours (4°C) and immersed in 15%, followed by 25% sucrose for cryoprotection. Brains were blocked in the coronal or sagittal planes and sectioned at 20 μm thickness using a cryostat. In each plane, one-in-eight serial sections were subjected to FLNa immunocytochemistry (ICC), and an adjacent series of sections was stained with cresyl violet. The others were used for double-labeling ICC.

FLNa ICC was performed on free-floating sections using standard avidin-biotin complex methods, as described previously (Chen et al., 2001). Briefly, after several washes with PBS containing 0.3% Triton X-100 (PBST; pH 7.4), sections were treated with 0.3% $H_2O_2$/PBS for 30 minutes, then blocked with 5% normal goat serum (NGS) for 30 minutes to prevent nonspecific binding. After being rinsed, sections were incubated for 36 hours at 4°C with rabbit anti-FLNa antiserum (Table 1) in PBS containing 1% BSA and washed in PBS-T (3 × 5 minutes). Sections were incubated with biotinylated goat anti-rabbit IgG (1:400; Vector Laboratories, Burlingame, CA) in PBS for 2 hours at room temperature. After being washed (3 ° 5 minutes), sections were incubated with the avidin-biotin-peroxidase complex solution (1:100; Vector Laboratories) for 3 hours, rinsed (3 × 5 minutes), and reacted with 0.04% 3,3′-diaminobenzidine (DAB) containing 0.01% $H_2O_2$.

Semiquantitative analysis was performed as previously reported (Chen et al., 2000), by counterstaining a subset of sections subjected to FLNa ICC with methyl green. The relative density of FLNa-ir neurons was expressed as the percentage of FLNa-positive neurons compared with the total number of methyl green-stained cells in the region of interest. Cell counting was performed under ×600 magnification, with the aid of a square lattice system over the entire area examined. For each animal, two to four sections per region were counted, and four rats in total were used to calculate the final density score. The density score was annotated as no positive cells (−), occasional (−/+, <10%), low (+, 10–25%), moderate (+, 25–50%), dense (+++, 50–75%), and very dense (++++, >75%) positive cells. Relative intensity of FLNa-ir labeling was evaluated based on the optical density of labeled cell bodies relative to background, using a gray level in the range of 0–255 (ImageTool). The intensity was scored as weakly positive (+, 0–60), moderately positive (++, 61–120), intensely positive (+++, 121–180), or strongly intense (++++, 181–255). The intensity values were consistent across the four brains tested; the final calculated values in Tables 2–4 represent mean intensity values.

Colabeling of FLNa with either MAP2 or PSD-95 was performed by using the tyramide signal amplification (TSA) technique (Chen et al., 2004). Sections were incubated overnight (4°C) with FLNa rabbit antiserum (1:10,000; Santa Cruz Biotechnology, Santa Cruz, CA), then treated with HRP conjugated anti-rabbit IgG (1:1,000; Perkin Elmer, Boston, MA) for 1.5 hours. Cy3-conjugated tyramide was diluted (1:150) in amplification buffer (Perkin Elmer, Boston, MA) and was applied in the dark for 5–6 minutes. After FLNa detection, sections were exposed to MAP2 or PSD-95 antiserum overnight at 4°C, and immunoreactivity was visualized by using anti-mouse IgG conjugated to Alexa-Fluor 488 (1:400; Invitrogen).

### *In situ* hybridization (ISH) and combined ISH/ICC

To detect FLNa mRNA *in situ*, digoxigenin (DIG)-3′-conjugated FLNa sense and antisense oligonucleotide probes were generated (Genscript, Piscataway, NJ). The anti-sense probe contained the sequence 5′-AGAAACAGACCTCAGCCTACTCACAGCCACTGT-3′, representing nucleotides 6073–6105 in the rat *FLNa* (NM_001134599.1). ISH of rat brain

slices was performed as previously described (Chen et al., 2001, 2004). Briefly, sections were washed with 2× saline sodium citrate (SSC: 0.3 M NaCl, 0.03M Na citrate) for 30 minutes, then subjected to an additional 30-minute incubation in a solution composed of 2× SSC/prehybridization solution (1:1). Prehybridization took place for 1 hour at 54°C in a humid chamber. The prehybridization solution consisted of 50% formamide, 4× SSC buffer, 5× Denhardt's solution, 5% dextran sulfate, 100 μg/ml yeast tRNA, and 100 μg/ml salmon sperm DNA. For hybridization, DIG-labeled probes were added, and sections were incubated at 54°C for 18 hours. For all steps, RNAse-free solutions, sterile slides, and six-well plates were used. After hybridization, sections were washed in 2× SSC at room temperature (2 × 15 minutes); 50% formamide/2× SSC at 65°C for 60 minutes; 50% formamide/0.1× SSC at 65°C for 60 minutes; and 0.1× and 0.05× SSC at 65°C, each for 30 minutes, and hybrid molecules were detected with an anti-DIG serum tagged with alkaline phosphatase according to the manufacturer's protocol (Roche, Indianapolis, IN). Chromogens consisted of 4-nitroblue tetrazolium chloride and 5-bromo-4-chloro-3-indolyl phosphate (Roche). The specificity of the hybridization reaction was verified by substituting labeled sense probe for the anti-sense probe and by omitting either the antisense probe or the alkaline phosphatase-conjugated antibody. No labeling was observed under these conditions.

For double labeling, free-floating sections were first processed for ISH according to the protocol described above. Sections were rinsed and then processed for FLNa-ICC as described above, with minor modifications: For visualization of FLNa immunoreaction, decreased concentrations of DAB (0.02%) and $H_2O_2$ (0.005%) were used. Sections were mounted on gelatin-coated slides, air dried, and sealed. To evaluate the possibility of altered sensitivity or specificity resulting from combined ISH/ICC, sections processed only for ICC or for ISH were compared with matched sections processed for double labeling. No differences in intensity and distribution of labeled cells were observed.

### Imaging and analysis

Brain sections were visualized on a Nikon Eclipse E400 epifluorescence microscope equipped with fluorescein, rhodamine, and DAPI/FITC/TRITC filter sets. Light microscopic images were obtained with a Nikon Digital Sight camera controlled by NIS-Elements F software (version 3.0; Nikon Instruments, Melville, NY). Confocal images were taken using an LSM-510 confocal microscope (Zeiss, Göottingen, Germany) with an Apochromat ×63 oil objective (numeric aperture = 1.40). Virtual z-sections of <1 μm were taken at 0.2–0.5-μm intervals. The image frame was digitized at 12 bits using a 1,024 × 1,024 pixel frame size. To prevent signal cross-talk (bleedthrough) in dual-labeling experiments, images were scanned sequentially (using the "multitrack" mode) by two separate excitation laser beams: an argon laser at a wavelength of 488 nm and an He/Ne laser at 543 nm. Z-stack reconstructions and final adjustments of image brightness were performed in ImageJ software (version 1.43; NIH).

## RESULTS

### Specificity of FLNa antibodies

Two separate antisera directed against epitopes at either the N′ or the C′ terminus of FLNa were used (Table 1). Both antisera recognized an approximately 280-kDa protein (Fig. 1A,D), in good agreement with the F1 expected molecular weight of FLNa. These antisera have been previously employed in Western blot and immunocytochemistry studies (e.g., Fox et al., 1998; Calderwood et al., 2001; Lu et al., 2006; E.J. Kim et al., 2007; Bastian et al., 2010), yielding specific bands at the appropriate molecular weights, which were absent in a cell line devoid of FLNa (Bachmann et al., 2006; Mammoto et al., 2007; E.J. Kim et al., 2007). As previously reported (Aakhus et al., 1989), additional and weaker bands were

observed using the N′ terminus-directed antibody, particularly an ~ 190-kDa band that has previously been identified as a calpain cleavage product of FLNa, located at the N′-terminal portion of the protein (Ezzel et al., 1988; Gorlin et al., 1990). Furthermore, developmental reduction in the specific 280-kDa band intensity was observed with either antibody when comparing brain extracts of different ages (Fig. 1), consistent with previous reports on the developmental regulation of FLNa protein and mRNA in the brain (Fox et al., 1998; Sheen et al., 2002). Immunocytochemical labeling of primary hippocampal neurons with either of the antibodies yielded similar distribution patterns (Fig. 1C,F), and no substantial signal was detected in samples devoid of the primary antibodies (not shown).

To further confirm the specificity of the FLNa antisera in brain tissue, we employed ISH in combination with ICC of FLNa. ISH of rat brain slices using an antisense nucleotide probe that targets the rat FLNa sequence (see Materials and Methods) yielded a positive signal across somata of many neuronal populations, supporting the presence of FLNa mRNA in these cells. In contrast, only a negligible signal was detected upon incubation with a control sense probe (Fig. 2A–C). The distribution pattern and relative intensity of ISH FLNa signal closely matched those of FLNa-ir as determined by ICC. For example, in the amygdala, relatively high levels of both FLNa mRNA and FLNa protein were detected in magnocellular cells of the basolateral nucleus, whereas much weaker signals (for both FLNa ISH and FLNa ICC) were found in the medial portion of the central nucleus and the basomedial nucleus (Fig. 2A,B; see also Fig. 5). In addition, ISH and ICC double labeling demonstrated the presence of both signals in individual neurons in various brain regions (Fig. 2D,E). Notably, whereas the ISH signal was limited to the soma, the FLNa-ir signal was typically observed in both soma and dendrites (Fig. 2F). Taken together, these results support the specificity of the FLNa antibodies used in this study and their suitability for the study of FLNa in the rat brain.

## Region-specific distribution of FLNa in the mature rat brain

FLNa-immunoreactive neurons were widely and selectively distributed throughout the rat brain. The density and intensity of FLNa signal were region and neuron specific. Detailed comparison of four different rat brains yielded essentially identical results, with only modest variations in labeling intensity. Below we provide a detailed description of FLNa region-specific immunoreactivity.

## Telencephalon

**Olfactory bulb—**In the olfactory bulb (Table 2, Fig. 3), mitral cells were intensely immunoreactive. Strongly labeled neurons were also present in the external, but not the internal, plexiform layer. In addition, many FLNa-ir puncta were found in the external plexiform layer and, rarely, in the internal plexiform layer. The granular layer contained numerous FLNa-ir puncta and a few weakly labeled neuronal somata. Most neurons in the anterior olfactory nucleus were FLNa positive. Within the olfactory tubercle, labeled neurons were prominent in the pyramidal layer. Scattered multipolar, intensely labeled neurons and some medium-sized, weakly labeled cells were seen in the polymorphic layer, but none were observed in the plexiform layer.

**Cerebral cortex—**Neocortical areas contained large numbers of FLNa-ir neurons. The most intensely labeled neurons were located in the cingulate cortex and in the somatosensory area of frontoparietal cortex, followed by the motor area of frontoparietal cortex and the temporal cortices. The laminar distribution of FLNa-ir neurons was striking: in the cingulate, frontoparietal, and most other neocortical regions, although FLNA-ir neurons were distributed throughout layers II–VI, maximal signal intensity was found in layers II and V, most notably in the frontoparietal cortex motor area (Fig. 3D–F). In the

entorhinal cortex, strongly labeled neurons were scattered in layers II, V, and VI, accompanied by many moderately labeled neurons.

**Hippocampus—**FLNa-ir neurons were most prominent in the pyramidal cell layer: The CA1 pyramidal cell layer was rich in moderately labeled puncta and contained several intensely labeled, large neurons. The CA2 region was distinguished by intense or moderate labeling of virtually all of pyramidal neurons. In CA3, maximal intensity of FLNa-ir was found in CA3a, with a gradual decline over CA3b and a fainter signal over CA3c. Outside of the pyramidal layer, only occasional medium-sized, multipolar or fusiform FLNa-ir neurons were scattered in strata oriens, lacunosum-moleculare, and radiatum (Fig. 4). Within the dentate gyrus, granule cell somata were outlined by a fine mesh of weakly stained puncta and accompanied by occasional strongly labeled basket-like neurons. Large, polymorphic, intensely labeled neurons were present in the hilus, whereas few FLNa-ir neurons were observed in the molecular layer (Fig. 4A,B). Most subicular pyramidal neurons were intensely labeled.

**Amygdala—**Large, intensely labeled neurons were widely distributed throughout the magnocellular and ventral regions of the basolateral nucleus (Fig. 5). In the central nucleus (ACe), weakly to moderately labeled neurons were found in medial and lateral divisions (Fig. 5B). The staining pattern of the medial nucleus consisted of weakly to moderately labeled medium-sized neurons, a pattern that was shared also by the basomedial nucleus: in both nuclei, the intensity of FLNa-ir signal was not uniform along the cell surface (Fig. 5C). Finally, weakly labeled neurons were present in the lateral nucleus as well as in the bed nucleus of stria terminalis (considered a part of the “extended amygdala”), where FLNa-ir neurons were abundant in both medial and lateral areas (Fig. 5).

**Basal forebrain and basal ganglia—**Most neurons in the lateral septum, particularly in the ventral and intermediate regions, had intense FLNa-ir signal, whereas neurons in the medial septal nucleus were moderately labeled (Fig. 6). The magnocellular neurons in both the horizontal and the vertical limbs of the diagonal band of Broca were moderately labeled. Neurons in the striatum (caudate-putamen) were not FLNa immunoreactive. Scattered weakly labeled neurons were apparent in the nucleus accumbens, whereas a large population of intensely labeled neurons was encountered in the globus pallidus and the ventral pallidum (Fig. 6).

## Diencephalon

**Habenula—**The medial habenula was characterized by densely immunoreactive neuropil and strongly labeled neurons (Table 3, Fig. 7A,B), whereas the lateral habenula showed scattered moderately labeled cells.

**Thalamus—**The anterior nuclear group contained abundant intensely labeled FLNa-ir neurons (in the anterodorsal and anteromedial nuclei) as well as moderately labeled ones (in the anteroventral nucleus). Most neurons in the lateral nuclear group, including the dorsal (laterodorsal; LD) and posterior nuclei, were weakly labeled. In the ventral group, intensely labeled neurons were abundant in the ventrolateral, ventromedial, and ventroposterior nuclei (Fig. 7C–E). Numerous moderately labeled neurons were also found in the thalamic reticular nucleus.

**Hypothalamus—**Within the paraventricular nucleus (PVN), parvocellular neurons demonstrated exceptionally intense FLNa-ir; in contrast, few positive neurons were present in the magnocellular division (Fig. 8A,B). Neurons in the dorsal hypothalamic area were generally strongly immunolabeled (Fig. 8C,D). In the ventromedial nucleus (VMH), neurons

were moderately labeled in both the dorsomedial and the ventrolateral parts, with scattered intensely labeled ones (Fig. 8C,E). FLNa-ir signal in the dorsomedial hypothalamic area was mostly weak (Fig. 8C).

### Brainstem and cerebellum

Strongly labeled FLNa-ir neurons were found in the pontine (Table 4, Fig. 9) and medullary raphe nuclei and in their mesencephalic counterparts. Within the reticular formation, large, intensely labeled FLNa-ir neurons were often seen in the pontine and gigantocellular reticular nuclei. The subcoeruleus region was rich in moderately labeled neurons, whereas neurons in the locus coeruleus were weakly labeled (Fig. 9B).

Within trigeminal nerve nuclei, large, multipolar neurons in the motor (Fig. 9C), principal sensory (Fig. 9B), and spinal subnuclei were intensely FLNa-ir. In the cochlear complex, the ventral nucleus had more intense labeling than the dorsal one. Some neurons in the facial, vagal, ambiguous, and hypoglossal nuclei were strongly FLNa-ir (not shown). Medium-sized, intensely labeled FLNa-ir neurons were often observed in both the medial and the lateral nuclei of the trapezoid body. In the superior olive, medium-sized FLNa-ir neurons were found (Fig. 9).

In the cerebellum, Purkinje cells were moderately FLNa-ir, whereas the granular and molecular layers contained only weakly labeled puncta (Fig. 9G). Large, multipolar neurons in the deep cerebellar nuclei were weakly stained, whereas the cerebellar white matter was devoid of FLNa immunoreactivity.

### Subcellular distribution of FLNa *in vitro* and *in vivo*

We employed mature hippocampal neurons grown in primary cultures to study the subcellular distribution of FLNa, taking advantage of the excellent amenability of these cells to optical imaging (Kaech and Banker, 2006). To evaluate the presence of FLNa in principal and inter-neuronal populations *in vitro*, we used an antibody directed against the interneuronal marker GAD65 (Table 1). FLNa-ir signal was detected in GAD65-negative, Pyramidal-shaped neurons (Fig. 10A–C), which formed the majority of neurons in culture (as previously reported; see Benson et al., 1994; Murphy et al., 1998; Noam et al., 2010). FLNa-ir signal was also detected in GAD65-positive neurons (Fig. 10D–F), indicating that FLNa expression is not selective for one of these classes of neurons. Examination of the subcellular distribution of FLNa revealed some-what stronger somatic FLNa-ir labeling than in dendrites. Somatic expression was characterized by punctate/clustered appearance (Fig. 11A,B), and a similar punctate signal was also found along dendrites, as shown by the colabeling of FLNa with the dendritic marker MAP2 (Fig. 11C–E). In light of the actin-binding properties of FLNa and the importance of actin as a backbone of dendritic spines, we asked whether dendritic FLNa is localized to dendritic spines. To hone in on potential localization of FLNa within synapses of dendritic spines, we colabeled FLNa with antibodies directed against either GluR1 (an ionotropic glutamate receptor localized to dendritic spines) or the postsynaptic marker PSD-95. Both procedures failed to detect significant FLNa signal in spines, indicating that dendritic FLNa is targeted primarily to the shaft (Fig. 11F–H).

Having established the subcellular distribution patterns of FLNa *in vitro*, we examined whether similar patterns occurred *in vivo*. We studied the distribution of FLNa in select neuronal populations of the rat brain with the additional use of dendritic and synaptic markers. Colabeling of FLNa with the dendritic marker MAP2 revealed FLNa-positive puncta that were scattered along the dendritic shaft of layer V neocortical neurons and hippocampal (CA1 and CA3) pyramidal neurons (Fig. 12). In line with the findings in

cultured neurons, *in vivo* dendritic FLNa did not colocalize with PSD-95-containing puncta (Fig. 13) and thus resided primarily in the dendritic shaft.

## DISCUSSION

In this study, we employed immunocytochemical techniques to characterize the expression and regional and subcellular distribution of the actin-binding protein FLNa in mature brain and cultured neurons. We report that 1) in the mature rat brain, FLNa is expressed across wide range of regions; 2) the distribution of FLNa is selective, as demonstrated by varying degrees of immunoreactive density and intensity across distinct neuronal populations; 3) FLNa is present in somata and along the dendrites of select neuronal populations; and 4) both *in vivo* and *in vitro*, dendritic FLNa-ir signal is distributed in puncta along the shaft and is minimally detected in spines.

The expression and function of FLNa has been extensively studied during early brain developmental stages, when FLNa plays important roles in neuronal migration (Feng and Walsh, 2004; Sarkisian et al., 2008; Carabalona et al., 2012). Indeed, high levels of brain FLNa are expressed in the pre- and perinatal period throughout the cerebral cortex and particularly within migrating neurons (Sheen et al., 2002). Although mRNA and protein levels of FLNa are downregulated during development (Sheen et al., 2002), moderate levels of FLNa have been consistently observed in adult brain (Fox et al., 1998; Petrecca et al., 2000; Sheen et al., 2002; Wang et al., 2008). Little is known on the precise roles of FLNa in mature neurons. By providing a comprehensive characterization of FLNa distribution across brain regions and in subcellular compartments, our data may reveal new leads to the potential functions of FLNa throughout life, including interaction with the actin transport machinery to facilitate localization of specific neuronal molecules. For example, both μ opioid and D2/D3 dopamine receptors are highly expressed in basal forebrain structures (Mansour et al., 1995; Arvidsson et al., 1995; Khan et al., 1998; Gurevich and Joyce, 1999; Seeman et al., 2006), and, in both cases, the expression is influenced by FLNa. Recently, interaction of FLNa with μ opioid receptors has been found to regulate G-protein binding of the receptor in the rat striatum (Wang et al., 2008). Indeed, our findings indicate strong FLNa-ir signal in lateral septum, ventral striatum, and ventral pallidum, areas where μ opioid receptors are expressed in high levels (Mansour et al., 1995). However, although μ opioid receptors are also abundant in the caudate-putamen, we could not detect FLNa-ir neurons in this region. These differences in distribution raise the intriguing possibility of region-specific regulation of μ opioid receptors by FLNa, which may be linked to altered function. A second molecular candidate to interact with FLNa in the mature CNS is dopamine receptors. Both D2 and D3 dopamine receptors have been shown to interact with FLNa in cultured cell lines (Li et al., 2000; Lin et al., 2001), but their interaction with FLNa in the brain (and the consequences of such interaction) remains to be explored. The expression of FLNa in striatal regions (Fig. 6) correlates with reported levels of D3 receptor expression: intense FLNa-ir signal was found in the ventral striatum, an area that contains relatively high levels of D3 dopamine receptors (Khan et al., 1998; Seeman et al., 2006), whereas no FLNa-ir was detected in the caudate-putamen region, which contains D2 but not D3 receptors (Levey et al., 1993; Khan et al., 1998; Seeman et al., 2006).

Additional intriguing distribution patterns emerged in the thalamus and hypothalamus. In thalamus, the most robust FLNa-ir signal was localized primarily to the anterodorsal nuclei, similar to the distribution of a known target of FLNa, the ion channel HCN1 (Santoro et al., 2000). In hypothalamus, FLNa-ir was abundant in parvocellular neurons and meager in magnocellular neurons of the paraventricular nucleus. The two cell populations synthesize and transport distinct peptides: parvocellular neurons project to the median eminence, and peptides are packaged and transported there in smaller vesicles (see, e.g., Swanson et al.,

1987), compared with the transport of magnocellular-neuron-derived vasopressin and oxytocin to the posterior pituitary. The distinctive distribution of FLNa-ir thus brings up the speculation that the protein might contribute selectively to one of these modes of peptide transport.

Both *in vitro* and *in vivo*, FLNa-ir was detected primarily in somata and along the apical dendritic shaft but was absent from spines. Dendritic spines are specialized compartments with a backbone of polymerized actin. The interaction of actin with a number of cellular proteins and enzymes is crucial to changes in spine shape and size and intrinsic processes of synaptic plasticity (Cingolani and Goda, 2008; Hotulainen and Hoogenraad, 2010). More specifically, several actin cross-linking proteins regulate spine morphology, which is typically characterized by partially bundled actin in the spine neck and a branched actin network in the spine head (Hotulainen and Hoogenraad, 2010). There is also evidence for different properties of the cytoskeleton within dendritic spines compared with the shaft (Hotulainen and Hoogenraad, 2010). In the context of this article, high FLNa concentrations promote stabilization and reduce dynamics of actin networks compared with actin networks that contain non-FLNa actin cross-linking proteins (Tseng et al., 2004). The exclusion of FLNa from spines, as we show here, is then logical; it allows the actin dynamics required for the changes of spine shape and size during processes of learning and memory (Chen et al., 2007). In contrast, the presence of FLNa in the shaft may contribute to actin stability.

Additional roles of FLNa in the dendritic shaft are supported by evidence for its interaction with several dendritic ion channels such as the potassium Kv4.2 (Petrecca et al., 2000), inward rectifying Kir2.1 (Sampson et al., 2003), and the nonselective hyperpolarization-activated HCN1 (Gravante et al., 2004). In all three types of ion channels, FLNa induced a clustered appearance of the channel on the cell surface, which was abolished in cells deficient in FLNa. However, whereas FLNa promotes the surface expression of Kir2.1 and Kv4.2 channels (Petrecca et al., 2000; Sampson et al., 2003), it seems to exert an opposite, inhibitory effect on HCN1 channels (Gravante et al., 2004). Future studies are required to determine whether FLNa directly regulates surface expression of these channels in neurons. FLNa might also play a role in the coregulation of different ion channels within the same dendrite.

Both *in vivo* and *in vitro* preparations were used in this work. *In vitro* systems such as the primary hippocampal neurons are inherently reduced and therefore cannot recapitulate the full properties of the living brain. However, primary neuronal cultures have been extremely beneficial for the basic study of neuronal processes: direct access for manipulation and good optical conditions made the primary hippocampal system widely popular in neuroscience research (Kaech and Banker, 2006). Our results demonstrate that the expression and subcellular distribution of FLNa in primary hippocampal neurons are comparable to those found *in vivo*, making this system adequate for future studies.

In summary, this study provides a detailed description of FLNa expression in the adult rat brain and in mature hippocampal neurons. The selective patterns found across brain regions and in distinct subcellular domains may provide important clues and several leads for future research on the roles of this actin-binding protein in regulating the structure and function of the mature brain.

## Acknowledgments

We thank Annie Koh, Seeta Rajpara, and Kristin Ng for technical assistance with Western blot analysis.

Grant sponsor: National Institutes of Health; Grant number: NS 35439; Grant number: NS 28912; Grant sponsor: Dutch National Epilepsy Foundation; Grant number: NEF 08.01.

## LITERATURE CITED


Aakhus AM, Wilkinson M, Pedersen TM, Solum NO. The use of PhastSystem crossed immunoelectrophoresis with immunoblotting to demonstrate a complex between glycoprotein Ib and the actin-binding protein (ABP) of human platelets. Electrophoresis. 1989; 10:758–761. [PubMed: 2612476]

Aizawa H, Kawasaki H, Murofushi H, Kotani S, Suzuki K, Sakai H. A common amino acid sequence in 190-kDa microtubule-associated protein and tau for the promotion of microtubule assembly. J Biol Chem. 1989; 264:5885–5890. [PubMed: 2494169]

Arvidsson U, Riedl M, Chakrabarti S, Lee JH, Nakano AH, Dado RJ, Loh HH, Law PY, Wessendorf MW, Elde R. Distribution and targeting of a mu-opioid receptor (MOR1) in brain and spinal cord. J Neurosci. 1995; 15:3328–3341. [PubMed: 7751913]

Bachmann AS, Howard JP, Vogel CW. Actin-binding protein filamin A is displayed on the surface of human neuroblastoma cells. Cancer Sci. 2006; 97:1359–1365. [PubMed: 16999820]

Bastian Y, Roa-Espitia AL, Mujica A, Hernandez-Gonzalez EO. Calpain modulates capacitation and acrosome reaction through cleavage of the spectrin cytoskeleton. Reproduction. 2010; 140:673–684. [PubMed: 20716611]

Benson DL, Watkins FH, Steward O, Banker G. Characterization of GABAergic neurons in hippocampal cell cultures. J Neurocytol. 1994; 23:279–295. [PubMed: 8089704]

Calderwood DA, Huttenlocher A, Kiosses WB, Rose DM, Woodside DG, Schwartz MA, Ginsberg MH. Increased filamin binding to beta-integrin cytoplasmic domains inhibits cell migration. Nat Cell Biol. 2001; 3:1060–1068. [PubMed: 11781567]

Carabalona A, Beguin S, Pallesi-Pocachard E, Buhler E, Pellegrino C, Arnaud K, Hubert P, Oualha M, Siffroi JP, Khantane S, Coupry I, Goizet C, Gelot AB, Represa A, Cardoso C. A glial origin for periventricular nodular heterotopia caused by impaired expression of filamin-A. Hum Mol Genet. 2012; 21:1004–1017. [PubMed: 22076441]

Chang YC, Gottlieb DI. Characterization of the proteins purified with monoclonal antibodies to glutamic acid decarboxylase. J Neurosci. 1988; 8:2123–2130. [PubMed: 3385490]

Chen LY, Rex CS, Casale MS, Gall CM, Lynch G. Changes in synaptic morphology accompany actin signaling during LTP. J Neurosci. 2007; 27:5363–5372. [PubMed: 17507558]

Chen Y, Brunson KL, Müller MB, Cariaga W, Baram TZ. Immunocytochemical distribution of corticotropin-releasing hormone receptor type-1 ($CRF_1$)-like immunoreactivity in the mouse brain: light microscopy analysis using an antibody directed against the C-terminus. J Comp Neurol. 2000; 420:305–323. [PubMed: 10754504]

Chen Y, Bender RA, Frotscher M, Baram TZ. Novel and transient populations of corticotropin-releasing hormone-expressing neurons in developing hippocampus suggest unique functional roles: a quantitative spatiotemporal analysis. J Neurosci. 2001; 21:7171–7181. [PubMed: 11549728]

Chen Y, Brunson KL, Adelmann G, Bender RA, Frotscher M, Baram TZ. Hippocampal corticotropin releasing hormone: pre- and postsynaptic location and release by stress. Neuroscience. 2004; 126:533–540. [PubMed: 15183503]

Cingolani LA, Goda Y. Actin in action: the interplay between the actin cytoskeleton and synaptic efficacy. Nat Rev Neurosci. 2008; 9:344–356. [PubMed: 18425089]

Das P, Lilly SM, Zerda R, Gunning WT 3rd, Alvarez FJ, Tietz EI. Increased AMPA receptor GluR1 subunit incorporation in rat hippocampal CA1 synapses during benzodiazepine withdrawal. J Comp Neurol. 2008; 511:832–846. [PubMed: 18924138]

Ezzel RM, Kenney DM, Egan S, Stossel TP, Hartwig JH. localization of the domain of actin-binding protein that binds to membrane glycoprotein Ib and actin in human platelets. J Biol Chem. 1988; 263:13303–13309. [PubMed: 3138234]

Feng Y, Walsh CA. The many faces of filamin: a versatile molecular scaffold for cell motility and signalling. Nat Cell Biol. 2004; 6:1034–1038. [PubMed: 15516996]

Fox JW, Lamperti ED, Eksioglu YZ, Hong SE, Feng Y, Graham DA, Scheffer IE, Dobyns WB, Hirsch BA, Radtke RA, Berkovic SF, Huttenlocher PR, Walsh CA. Mutations in filamin 1 prevent

migration of cerebral cortical neurons in human periventricular heterotopia. Neuron. 1998; 21:1315–1325. [PubMed: 9883725]

Gorlin JB, Yamin R, Egan S, Stewart M, Stossel TP, Kwiatkowski DJ, Hartwig JH. Human endothelial actin-binding protein (ABP280, nonmuscle filamin): a molecular leaf spring. J Cell Biol. 1990; 111:1089–1105. [PubMed: 2391361]

Gravante B, Barbuti A, Milanesi R, Zappi I, Viscomi C, DiFrancesco D. Interaction of the pacemaker channel HCN1 with filamin A. J Biol Chem. 2004; 279:43847–43853. [PubMed: 15292205]

Gurevich EV, Joyce JN. Distribution of dopamine D3 receptor expressing neurons in the human forebrain: comparison with D2 receptor expressing neurons. Neuropsychopharmacology. 1999; 20:60–80. [PubMed: 9885786]

Hotulainen P, Hoogenraad CC. Actin in dendritic spines: connecting dynamics to function. J Cell Biol. 2010; 189:619–629. [PubMed: 20457765]

Huber G, Matus A. Differences in the cellular distributions of two microtubule-associated proteins, MAP1 and MAP2, in rat brain. J Neurosci. 1984; 4:151–160. [PubMed: 6198491]

Kaech S, Banker G. Culturing hippocampal neurons. Nat Protoc. 2006; 1:2406–2415. [PubMed: 17406484]

Khan ZU, Gutierrez A, Martin R, Penafiel A, Rivera A, De La Calle A. Differential regional and cellular distribution of dopamine D2-like receptors: an immunocytochemical study of subtype-specific antibodies in rat and human brain. J Comp Neurol. 1998; 402:353–371. [PubMed: 9853904]

Kim EJ, Park JS, Um SJ. Filamin A negatively regulates the transcriptional activity of p73alpha in the cytoplasm. Biochem Biophys Res Commun. 2007; 362:1101–1106. [PubMed: 17825253]

Kim EY, Ridgway LD, Dryer SE. Interactions with filamin A stimulate surface expression of large-conductance $Ca^{2+}$-activated $K^{+}$ channels in the absence of direct actin binding. Mol Pharmacol. 2007; 72:622–630. [PubMed: 17586600]

King AE, Chung RS, Vickers JC, Dickson TC. Localization of glutamate receptors in developing cortical neurons in culture and relationship to susceptibility to excitotoxicity. J Comp Neurol. 2006; 498:277–294. [PubMed: 16856139]

Koulen P, Fletcher EL, Craven SE, Bredt DS, Wäassle H. Immunocytochemical localization of the postsynaptic density protein PSD-95 in the mammalian retina. J Neurosci. 1998; 18:10136–10149. [PubMed: 9822767]

Kornau HC, Schenker LT, Kennedy MB, Seeburg PH. Domain interaction between NMDA receptor subunits and the postsynaptic density protein PSD-95. Science. 1995; 269:1737–1740. [PubMed: 7569905]

Lepousez G, Csaba Z, Bernard V, Loudes C, Videau C, Lacombe J, Epelbaum J, Viollet C. Somatostatin interneurons delineate the inner part of the external plexiform layer in the mouse main olfactory bulb. J Comp Neurol. 2010; 518:1976–1994. [PubMed: 20394054]

Levey AI, Hersch SM, Rye DB, Sunahara RK, Niznik HB, Kitt CA, Price DL, Maggio R, Brann MR, Ciliax BJ. Localization of D1 and D2 dopamine receptors in brain with subtype-specific antibodies. Proc Natl Acad Sci U S A. 1993; 90:8861–8865. [PubMed: 8415621]

Li M, Bermak JC, Wang ZW, Zhou QY. Modulation of dopamine D(2) receptor signaling by actin-binding protein (ABP-280). Mol Pharmacol. 2000; 57:446–452. [PubMed: 10692483]

Lim ST, Lim KC, Giuliano RE, Federoff HJ. Temporal and spatial localization of nectin-1 and l-afadin during synaptogenesis in hippocampal neurons. J Comp Neurol. 2008; 507:1228–1244. [PubMed: 18181141]

Lin R, Karpa K, Kabbani N, Goldman-Rakic P, Levenson R. Dopamine D2 and D3 receptors are linked to the actin cytoskeleton via interaction with filamin A. Proc Natl Acad Sci U S A. 2001; 98:5258–5263. [PubMed: 11320256]

Lu J, Tiao G, Folkerth R, Hecht J, Walsh C, Sheen V. Overlapping expression of ARFGEF2 and filamin A in the neuroependymal lining of the lateral ventricles: insights into the cause of periventricular heterotopia. J Comp Neurol. 2006; 494:476–484. [PubMed: 16320251]

Mammoto A, Huang S, Ingber DE. Filamin links cell shape and cytoskeletal structure to Rho regulation by controlling accumulation of p190RhoGAP in lipid rafts. J Cell Sci. 2007; 120:456–467. [PubMed: 17227794]

Mansour A, Fox CA, Burke S, Akil H, Watson SJ. Immunohistochemical localization of the cloned mu opioid receptor in the rat CNS. J Chem Neuroanat. 1995; 8:283–305. [PubMed: 7669273]

Murphy DD, Cole NB, Greenberger V, Segal M. Estradiol increases dendritic spine density by reducing GABA neurotransmission in hippocampal neurons. J Neurosci. 1998; 18:2550–2559. [PubMed: 9502814]

Nakamura F, Osborn TM, Hartemink CA, Hartwig JH, Stossel TP. Structural basis of filamin A functions. J Cell Biol. 2007; 179:1011–1025. [PubMed: 18056414]

Nakamura F, Stossel TP, Hartwig JH. The filamins: organizers of cell structure and function. Cell Adhesion Migration. 2011; 5:160–169. [PubMed: 21169733]

Noam Y, Zha Q, Phan L, Wu RL, Chetkovich DM, Wadman WJ, Baram TZ. Trafficking and surface expression of hyperpolarization-activated cyclic nucleotide-gated channels in hippocampal neurons. J Biol Chem. 2010; 285:14724–14736. [PubMed: 20215108]

Onoprishvili I, Andria ML, Kramer HK, Ancevska-Taneva N, Hiller JM, Simon EJ. Interaction between the mu opioid receptor and filamin A is involved in receptor regulation and trafficking. Mol Pharmacol. 2003; 64:1092–1100. [PubMed: 14573758]

Pak CW, Flynn KC, Bamburg JR. Actin-binding proteins take the reins in growth cones. Nat Rev Neurosci. 2008; 9:136–147. [PubMed: 18209731]

Parrini E, Ramazzotti A, Dobyns WB, Mei D, Moro F, Veggiotti P, Marini C, Brilstra EH, Dalla Bernardina B, Goodwin L, Bodell A, Jones MC, Nangeroni M, Palmeri S, Said E, Sander JW, Striano P, Takahashi Y, Van Maldergem L, Leonardi G, Wright M, Walsh CA, Guerrini R. Periventricular heterotopia: phenotypic heterogeneity and correlation with filamin A mutations. Brain. 2006; 129:1892–1906. [PubMed: 16684786]

Petrecca K, Miller DM, Shrier A. Localization and enhanced current density of the Kv4.2 potassium channel by interaction with the actin-binding protein filamin. J Neurosci. 2000; 20:8736–8744. [PubMed: 11102480]

Popowicz GM, Schleicher M, Noegel AA, Holak TA. Filamins: promiscuous organizers of the cytoskeleton. Trends Biochem Sci. 2006; 31:411–419. [PubMed: 16781869]

Rostkowski AB, Teppen TL, Peterson DA, Urban JH. Cell-specific expression of neuropeptide Y Y1 receptor immunoreactivity in the rat basolateral amygdala. J Comp Neurol. 2009; 517:166–176. [PubMed: 19731317]

Sampson LJ, Leyland ML, Dart C. Direct interaction between the actin-binding protein filamin-A and the inwardly rectifying potassium channel, Kir2.1. J Biol Chem. 2003; 278:41988–41997. [PubMed: 12923176]

Santoro B, Chen S, Luthi A, Pavlidis P, Shumyatsky GP, Tibbs GR, Siegelbaum SA. Molecular and functional heterogeneity of hyperpolarization-activated pacemaker channels in the mouse CNS. J Neurosci. 2000; 20:5264–5275. [PubMed: 10884310]

Sarkisian MR, Bartley CM, Rakic P. Trouble making the first move: interpreting arrested neuronal migration in the cerebral cortex. Trends Neurosci. 2008; 31:54–61. [PubMed: 18201775]

Seeman P, Wilson A, Gmeiner P, Kapur S. Dopamine D2 and D3 receptors in human putamen, caudate nucleus, and globus pallidus. Synapse. 2006; 60:205–211. [PubMed: 16739118]

Sheen VL, Feng Y, Graham D, Takafuta T, Shapiro SS, Walsh CA. Filamin A and filamin B are co-expressed within neurons during periods of neuronal migration and can physically interact. Hum Mol Genet. 2002; 11:2845–2854. [PubMed: 12393796]

Sheen VL, Jansen A, Chen MH, Parrini E, Morgan T, Ravenscroft R, Ganesh V, Underwood T, Wiley J, Leventer R, Vaid RR, Ruiz DE, Hutchins GM, Menasha J, Willner J, Geng Y, Gripp KW, Nicholson L, Berry-Kravis E, Bodell A, Apse K, Hill RS, Dubeau F, Andermann F, Barkovich J, Andermann E, Shugart YY, Thomas P, Viri M, Veggiotti P, Robertson S, Guerrini R, Walsh CA. Filamin A mutations cause periventricular heterotopia with Ehlers-Danlos syndrome. Neurology. 2005; 64:254–262. [PubMed: 15668422]

Stossel TP, Condeelis J, Cooley L, Hartwig JH, Noegel A, Schleicher M, Shapiro SS. Filamins as integrators of cell mechanics and signalling. Nat Rev Mol Cell Biol. 2001; 2:138–145. [PubMed: 11252955]

Swanson LW, Sawchenko PE, Lind RW, Rho JH. The CRH motoneuron: differential peptide regulation in neurons with possible synaptic, paracrine, and endocrine outputs. Ann N Y Acad Sci. 1987; 512:12–23. [PubMed: 3327422]

Tseng Y, An KM, Esue O, Wirtz D. The bimodal role of filamin in controlling the architecture and mechanics of F-actin networks. J Biol Chem. 2004; 279:1819–1826. [PubMed: 14594947]

Wang HY, Frankfurt M, Burns LH. High-affinity naloxone binding to filamin a prevents mu opioid receptor-Gs coupling underlying opioid tolerance and dependence. PLoS One. 2008; 3:e1554. [PubMed: 18253501]

Wenthold RJ, Yokotani N, Doi K, Wada K. Immunochemical characterization of the non-NMDA glutamate receptor using subunit-specific antibodies. Evidence for a hetero-oligomeric structure in rat brain. J Biol Chem. 1992; 267:501–507. [PubMed: 1309749]

Yamamoto T, Yamato E, Tashiro F, Sato E, Noso S, Ikegami H, Tamura S, Yanagawa Y, Miyazaki JI. Development of autoimmune diabetes in glutamic acid decarboxylase 65 (GAD65) knockout NOD mice. Diabetologia. 2004; 47:221–224. [PubMed: 14676944]

Zamanillo D, Sprengel R, Hvalby O, Jensen V, Burnashev N, Rozov A, Kaiser KM, Koster HJ, Borchardt T, Worley P, Lubke J, Frotscher M, Kelly PH, Sommer B, Andersen P, Seeburg PH, Sakmann B. Importance of AMPA receptors for hippocampal synaptic plasticity but not for spatial learning. Science. 1999; 284:1805–1811. [PubMed: 10364547]

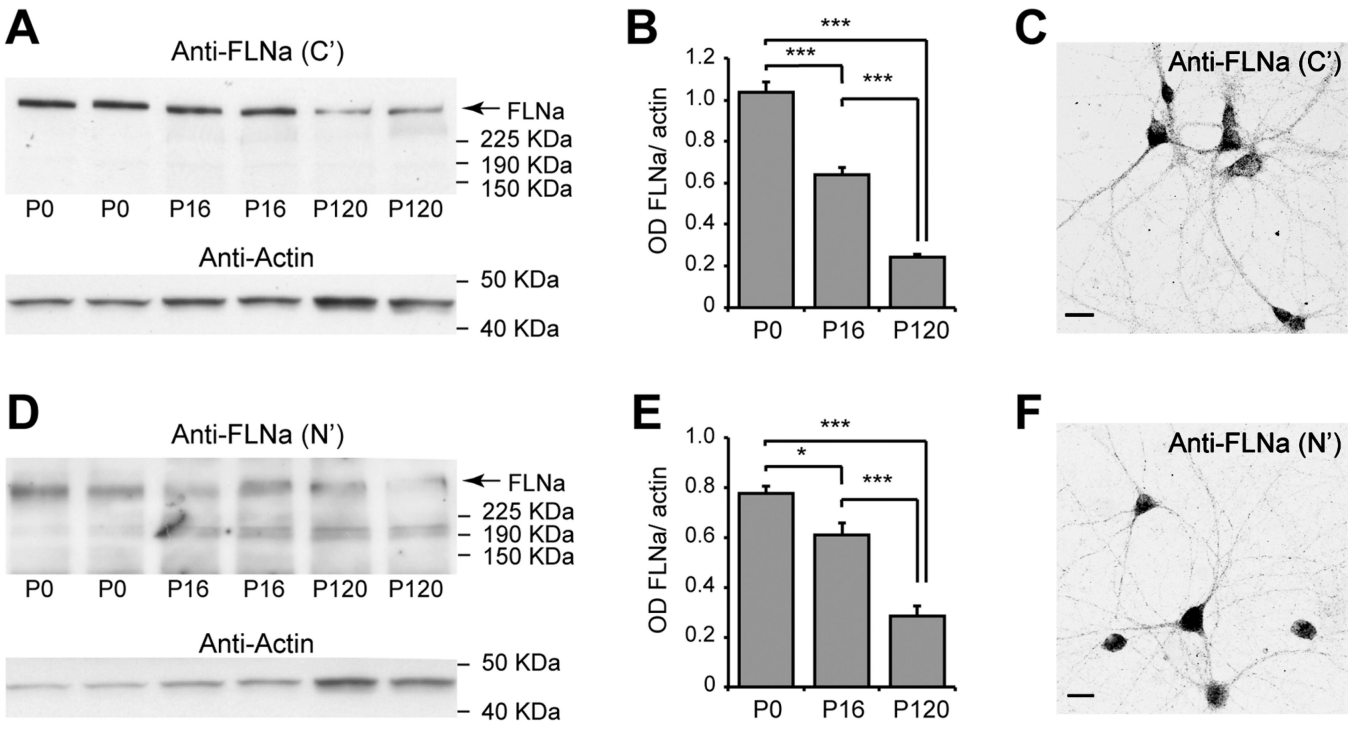


**Figure 1.**

Specificity of FLNa antibodies used in this study. **A,D:** Western blot gels of rat whole-brain extracts, demonstrating selective bands at the expected molecular weight of FLNa (280 kDa). Two different antibodies were used, directed against either the C′ (A) or the N′ (D) terminus of the protein. The typical decline in FLNa protein levels during brain development is shown by using animals from three age groups, as indicated (P, postnatal day). For each age group, two animals were used (represented by two separate lanes). **B,E:** Quantification of Western blot band intensities for the C′ (B) and N′ (E) terminus FLNa antisera. Statistical significance was determined by using one-way ANOVA ($P < 0.001$) followed by Tukey *post hoc* test (*$P < 0.05$, ***$P < 0.001$; n = 4 animals per age group). Optical densities (OD) were determined by using gel images at exposure times that produced OD values within the linear response range (normally 0.2–0.8OD). **C,F:** Immunolabeling of primary hippocampal cultures (3–4 weeks *in vitro*) showing positive signal and similar distribution patterns for both antibodies. Scale bars = 20 μm.

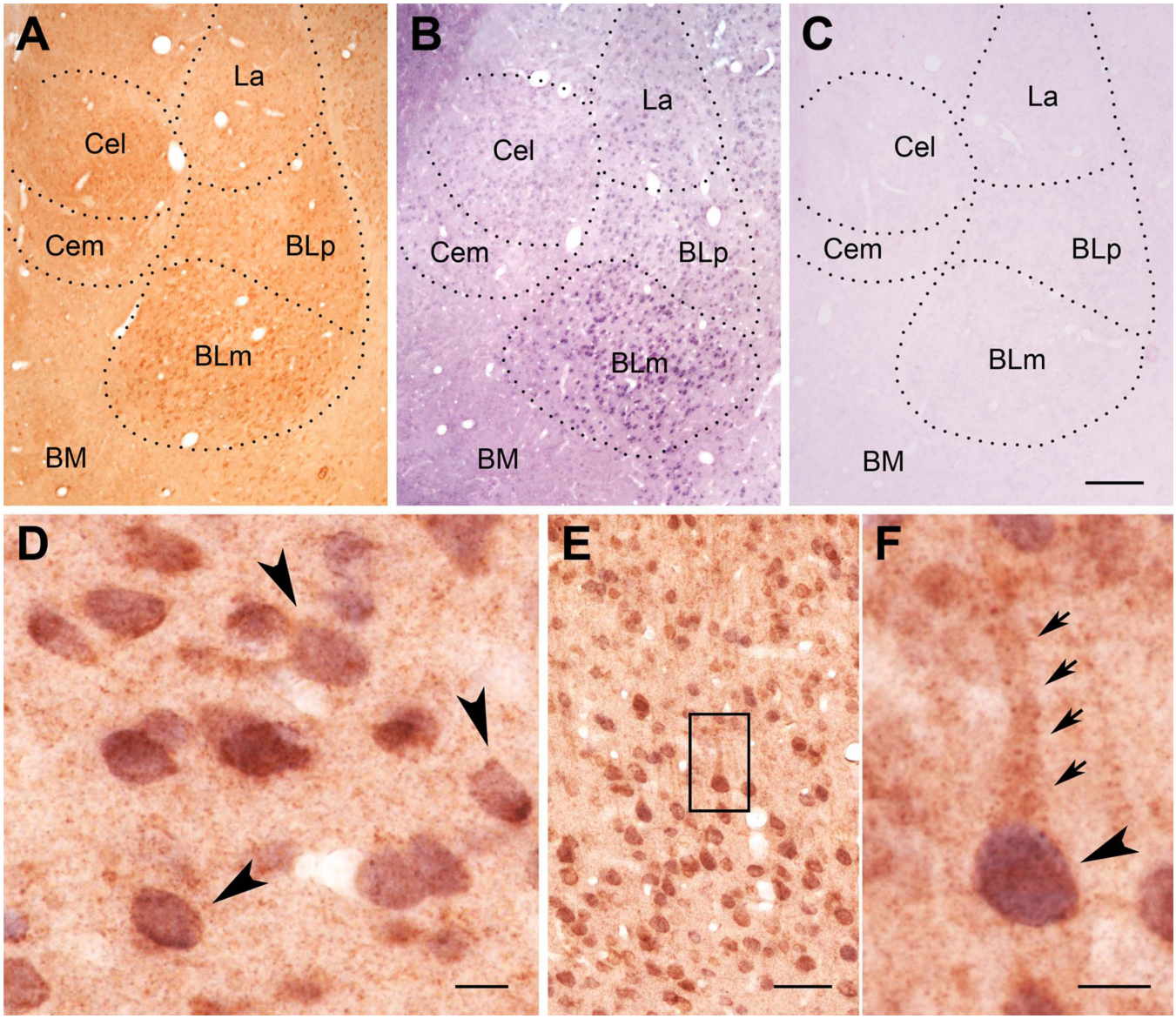


**Figure 2.**

Comparison of FLNa mRNA and protein distribution in adult rat brain. **A,B:** FLNa-ir and ISH signals in the amygdala. The pattern of FLNa-ir signal (A) closely matched that of FLNa ISH (B), with the strongest labeling at the magnocellular basolateral nucleus (BLm) and weaker signal in the medial central (Cem) and basomedial (BM) nuclei. Only negligible signal was detected using a control sense probe (**C**). **D:** Double labeling of FLNa in neurons of the basolateral amygdaloid nucleus, using combined ICC (brown) and ISH (purple), confirmed the presence of both FLNa mRNA and protein in the same neurons (arrowheads). **E,F:** ISH and ICC double labeling of FLNa in the neocortex. Boxed area in E denotes area magnified in F, demonstrating the presence of FLNa-ir in both soma (arrowhead) and apical dendrites (arrows; see also Fig. 3E,F), whereas ISH signal was localized to the soma only. Brain slices are of 3-month-old rats. Scale bars = 450 μm in C (applies to A–C); 20 μm in D,F; 100 μm in E.

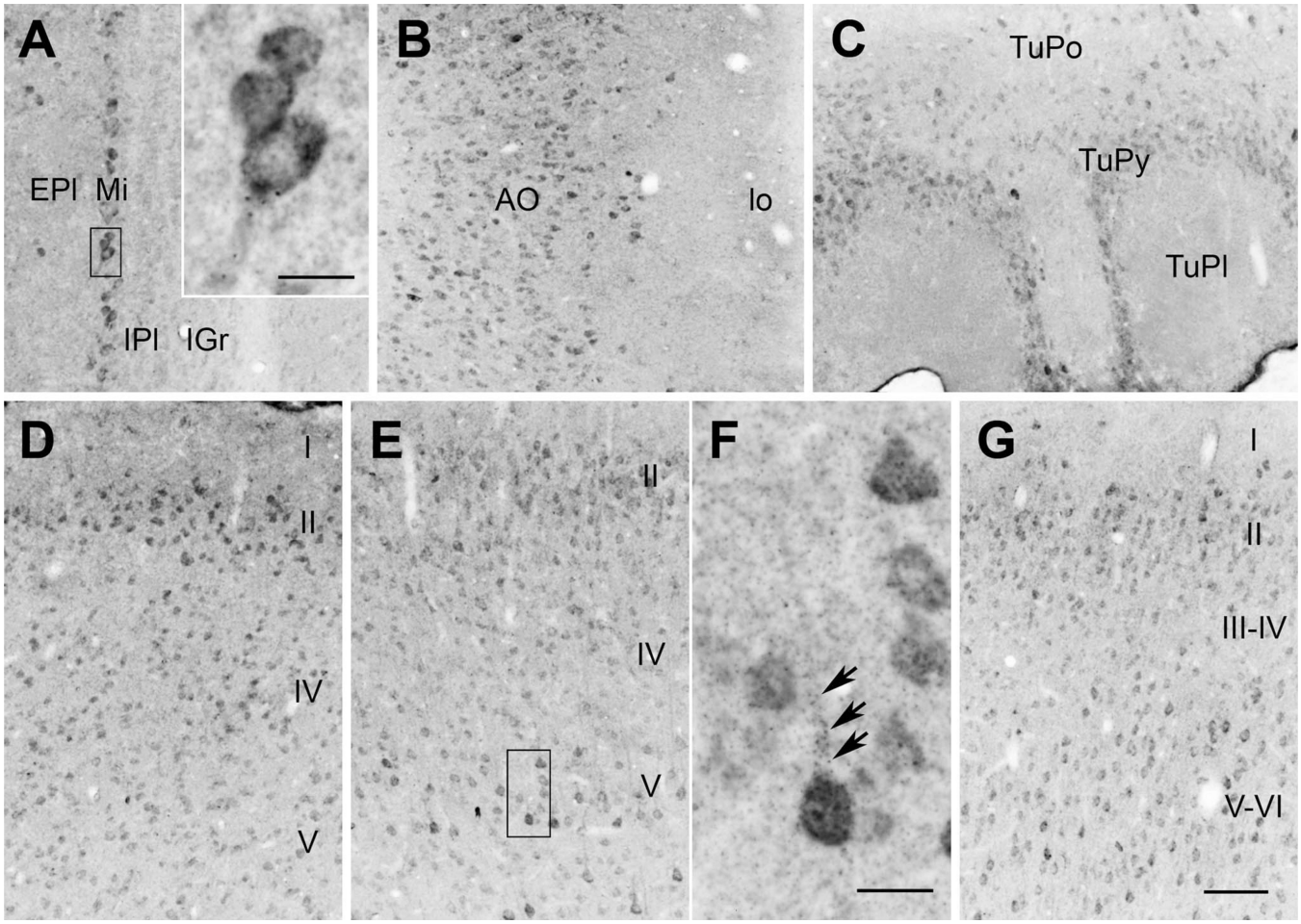


**Figure 3.**

Expression of FLNa in olfactory and cortical regions. **A–C:** FLNa immunoreactivity in olfactory bulb (A), anterior olfactory nucleus (B), and olfactory tubercle (C). **Inset** shows intensely labeled mitral cells in the mitral cell layer (Mi). EPl and IPl, external and internal plexiform layers, respectively; IGr, internal granular layer; lo, lateral olfactory tract; AO, anterior olfactory nucleus; TuPo, TuPy, and TuPl, polymorphic, pyramidal, and plexiform layer of olfactory tubercles, respectively. **D–G:** Distribution of FLNa in frontal cortex (D), neocortex (E,F), and entorhinal cortex (G). Boxed area in E denotes area magnified in F, showing strongly labeled somata of layer V pyramidal neurons, as well as FLNa-positive puncta along the primary dendritic branch (arrows). Cortical layers are denoted by Roman numerals. Scale bars = 100 μm in G (applies to A–E,G); 20 μm in inset,F.

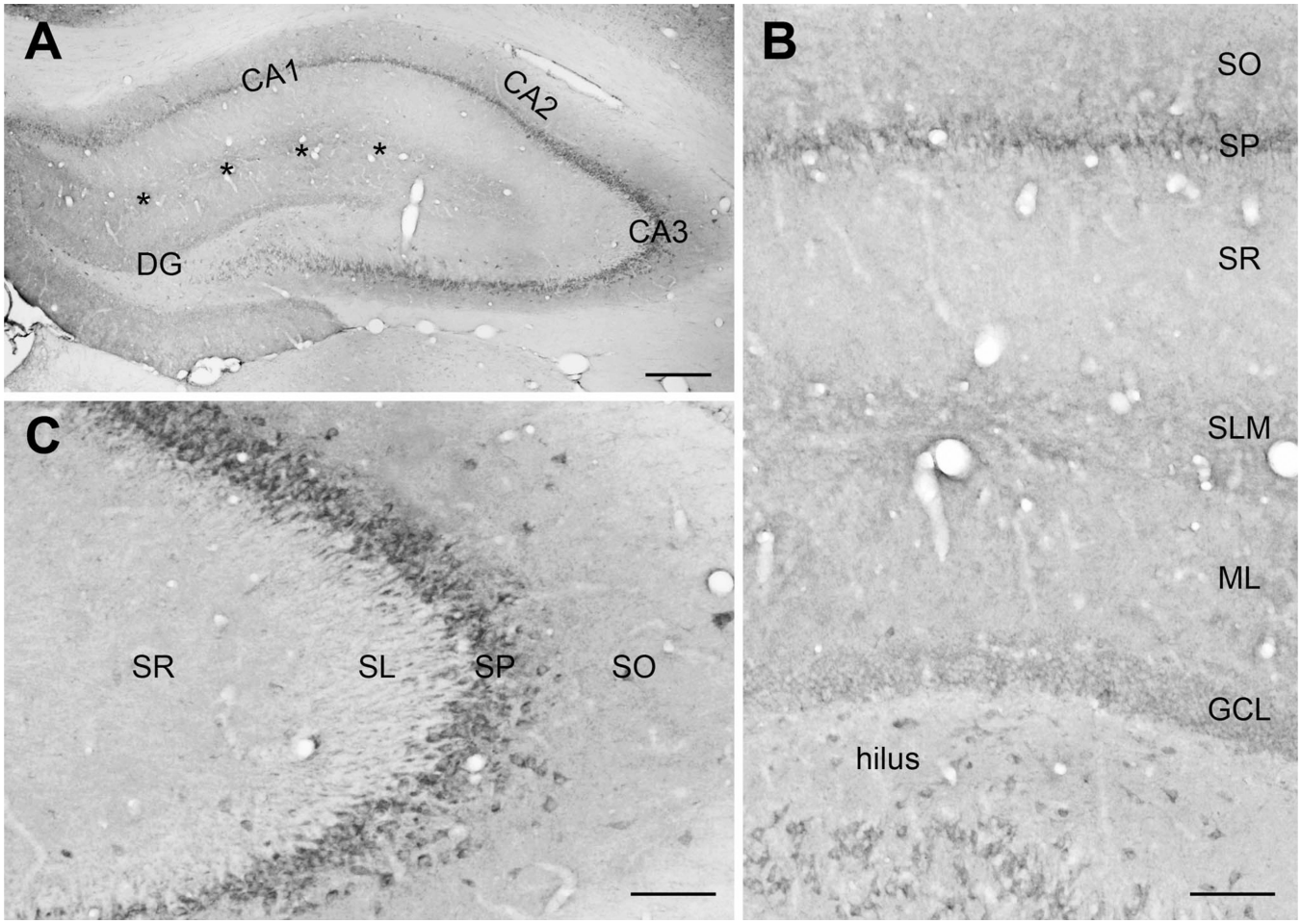


**Figure 4.**

Distribution of FLNa in the hippocampus (**A**). Pyramidal neurons in CA1 area (**B**) were weakly labeled when compared with those in CA3 area (**C**). Most CA3 pyramidal neurons had intense signal, particularly in the CA3a subregion. Within the dentate gyrus (DG), granule cell somata were outlined by a fine mesh of weakly stained puncta, and strong labeling was found in hilar neurons (B). Asterisks demarcate the hippocampal fissure; SO, SP, SR, SL, SLM, stratum oriens, pyramidale, radiatum, lucidum, and lacunosum-moleculare, respectively; ML, molecular layer of DG; GCL, granule cell layer. Scale bars = 200 μm in A; 100 μm in B,C.

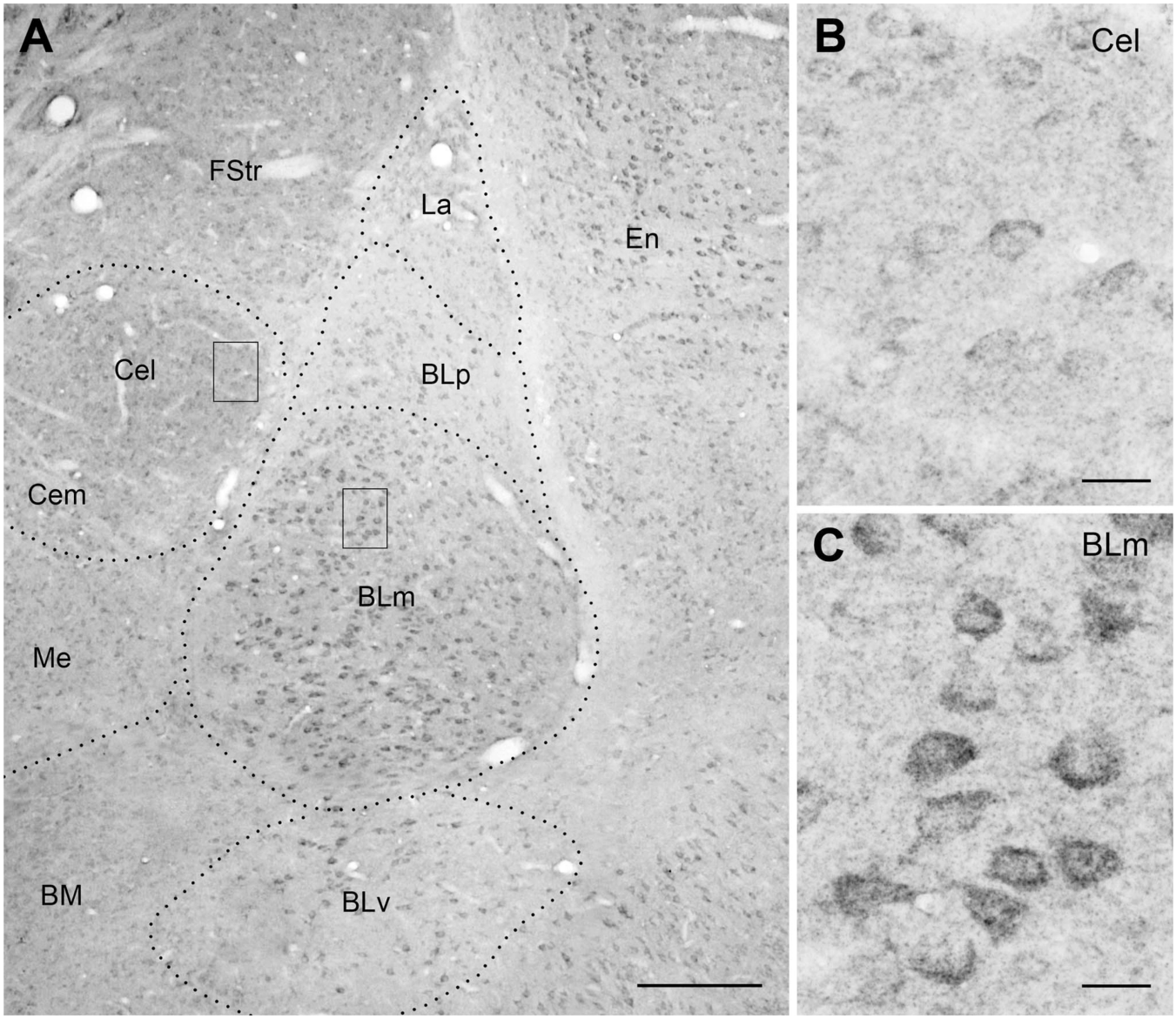


**Figure 5.**

Distribution of FLNa-ir neurons in the amygdala (**A**) and morphology of FLNa-ir neurons in the boxed areas in the central (**B**) and basolateral (**C**) amygdaloid nuclei. In the central nucleus, whereas neurons in the lateral division (Cel) are moderately labeled, the medial (Cem) neurons are weakly stained. Intensely labeled neurons are presented throughout the magnocellular (BLm) and ventral (BLv) divisions of basolateral nucleus. Within the medial (Me) and basomedial (BM) nuclei, FLNa distribution was typically nonhomogenous in somata. FStr, fundus striati; En, entorhinal cortex; La, lateral amygdaloid nucleus. Scale bars = 300 μm in A; 20 μm in B,C.

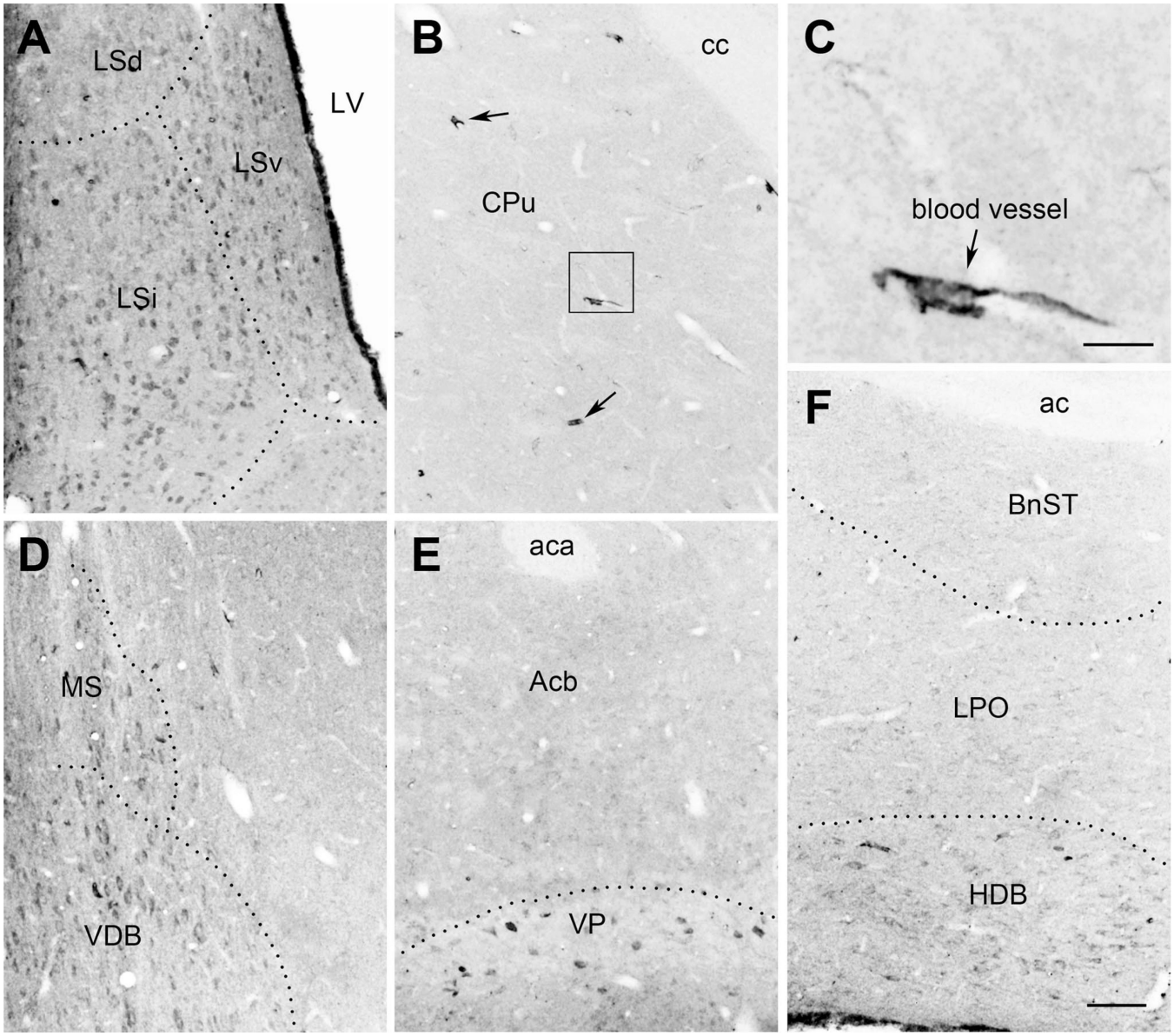


**Figure 6.**

Distribution of FLNa in septum, caudate-putamen, and other basal forebrain structures. **A:** In the lateral septum, intense labeling was evident in the ventral (LSv) and intermediate (LSi) parts, whereas only a few neurons in the dorsal part (LSd) were moderately labeled. **B:** Neuronal FLNa expression was not detected in the caudate-putamen (CPu), although some blood vessels (arrows) were strongly labeled. **C:** A magnified blood vessel from the boxed area in B. **D:** Strongly labeled neurons are scattered in both the medial septal nucleus (MS) and the vertical limb of the nucleus of the diagonal band of Broca (VDB), where most neurons are moderately labeled. **E:** FLNa-ir neurons in the basal ganglia, including the accumbens nucleus (Acb) and ventral striatum or pallidum (VP). Weakly labeled neurons were occasionally detected in Acb, whereas neurons in VP were intensely stained. F: Neurons in the bed nucleus of the stria terminalis (BnST) and horizontal limb of the diagonal band (HDB) are weakly and moderately labeled, respectively. LV, lateral ventricle;

aca, anterior part of anterior commissure; ac, anterior commissure; cc, corpus callosum; LPO, lateral preoptic area. Scale bars = 100 μm in F (applies to A,B,D–F); 20 μm in C.

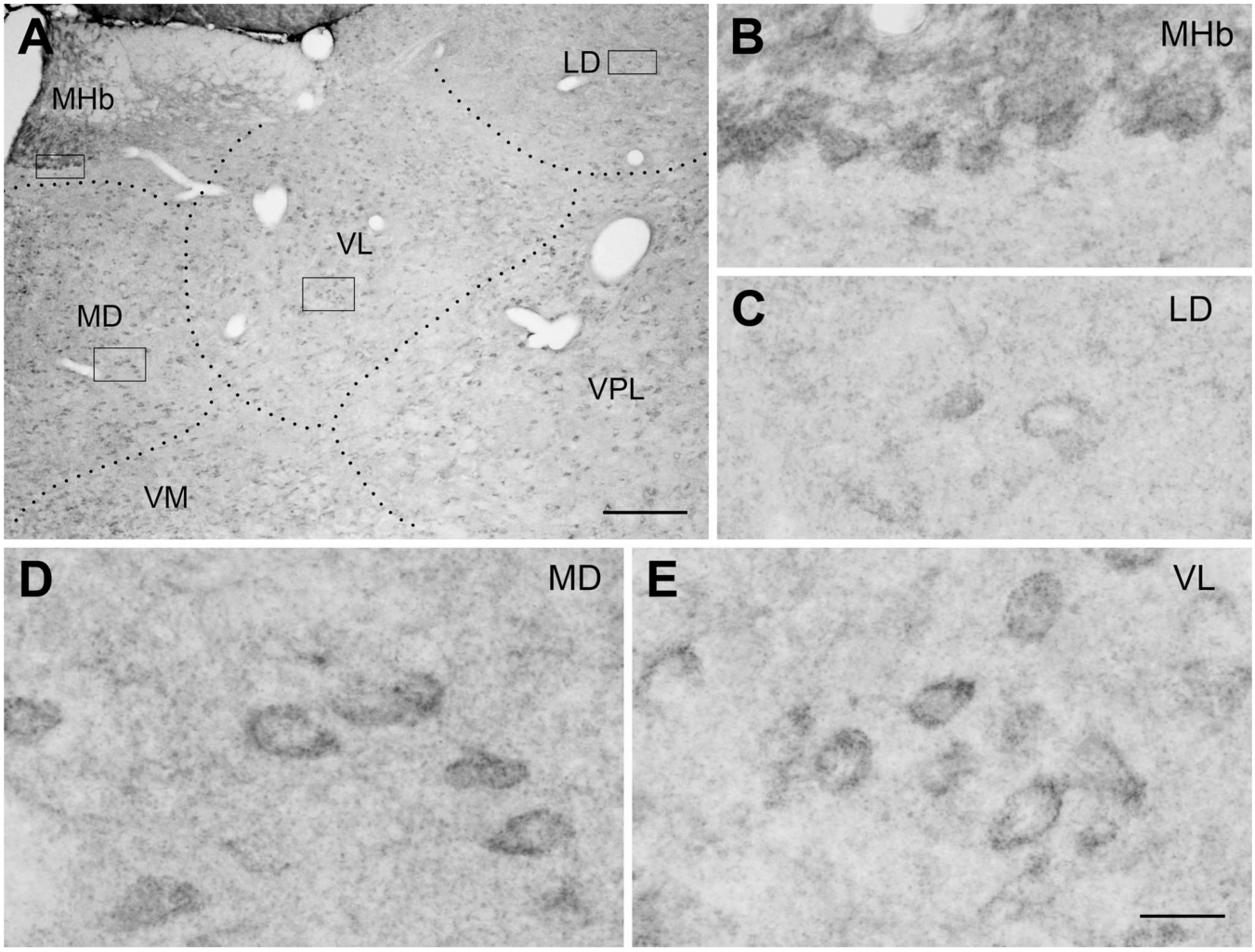


**Figure 7.**

Distribution of FLNa in the thalamus. Boxed areas in **A** are magnified in **B–E** to show the immunoreactive neurons in the medial habenular nucleus (MHb), and the laterodorsal (LD), mediodorsal (MD), and ventrolateral (VL) thalamic nuclei. VM and VPL, ventromedial and lateral part of ventroposterior thalamic nucleus, respectively. Scale bars = 250 μm in A; 20 μm in E (applies to B–E).

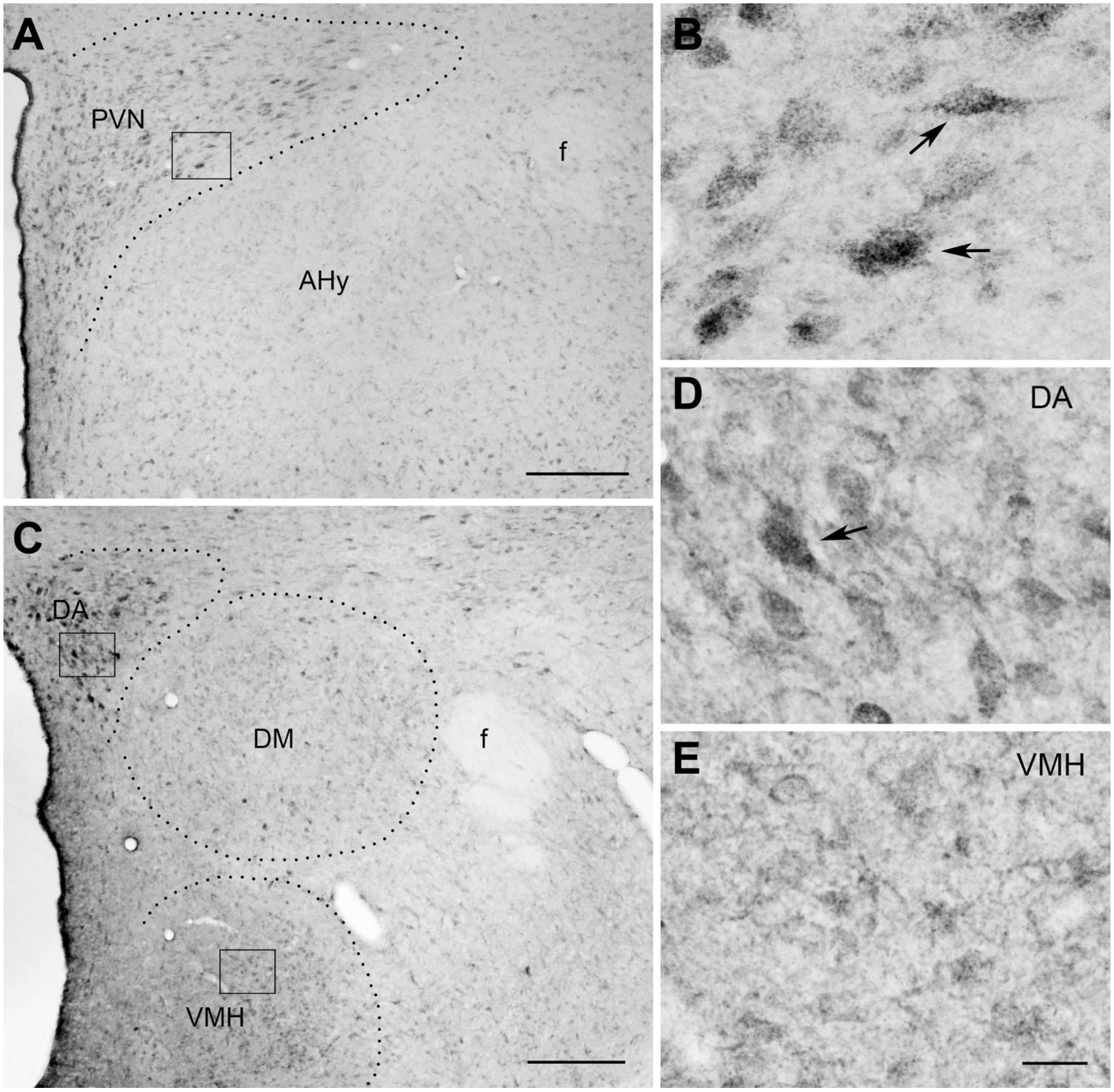


**Figure 8.**

Distribution of FLNa in the hypothalamic areas. **A,B:** FLNa-ir neurons in the paraventricular nucleus (PVN). Boxed area in A was magnified in B, showing strong labeling of parvocellular neurons in the PVN (arrows). **C–E:** Neurons in the dorsal hypothalamic area (DA) were frequently intensely labeled. A few strongly labeled neurons were also scattered in the ventromedial (VMH) and dorsomedial (DM) hypothalamic areas as well as in the anterior hypothalamic area (AHy), where the majority of medium-sized neurons were weakly or moderately labeled. Boxed areas in C are magnified in D and E to present the morphology of FLNa-positive neurons in DA and VMH, respectively. f, Fornix. Scale bars = 250 μm in A,C; 20 μm in E (applies to B,D,E).

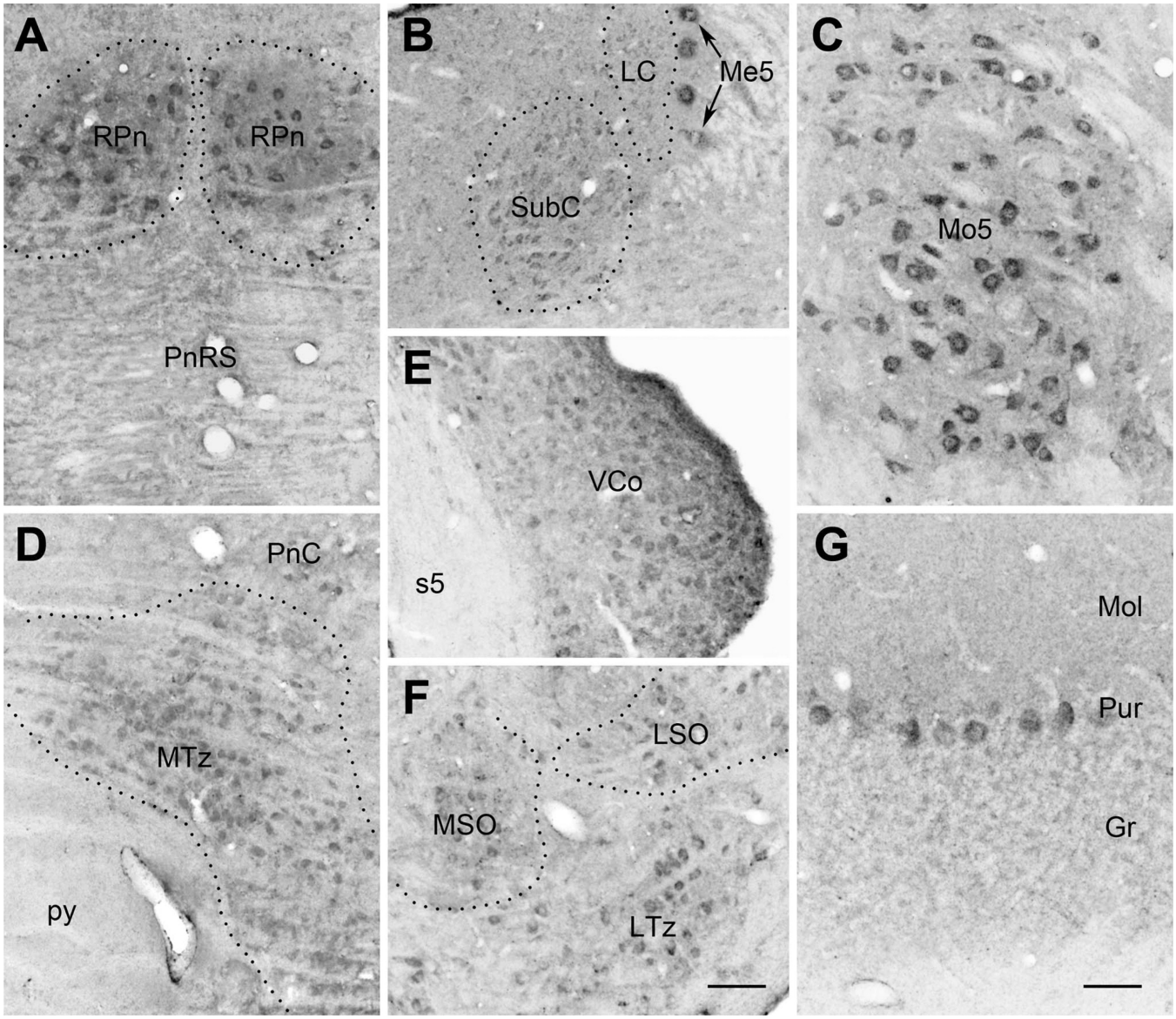


**Figure 9.**

Immunoreactivity of FLNa in brainstem nuclei and cerebellum. **A:** Strongly labeled, FLNa-ir neurons in the raphe pontis nucleus (RPn). PnRS, pontine reticular structure. **B:** Neurons of the mesencephalic nucleus of trigeminal nerve (Me5) were intensely labeled, whereas most medium-sized neurons in the subcoeruleus (SubC) were moderately labeled, and neurons in the locus coeruleus (LC) were weakly labeled. **C:** Motoneurons in the motor trigeminal nucleus (Mo5), showing the strongest labeling seen in the brainstem. **D–F** show the distribution of FLNa in neurons of the medial nucleus of trapezoid body (MTz), ventral cochlear nuclei (VCo), and medial and lateral superior olive (MSO and LSO, respectively). PnC, pontine reticular nucleus; py, pyramidal tract; s5, sensory root of trigeminal nerve; LTz, lateral nucleus of trapezoid body. **G:** Within the cerebellum, Purkinje cells (Pur) are moderately labeled. The granular layer (Gr) as well as the molecular layer region (Mol) contained numerous weakly labeled puncta. Scale bars = 100 μm in F (applies to A–F); 50 μm in G.

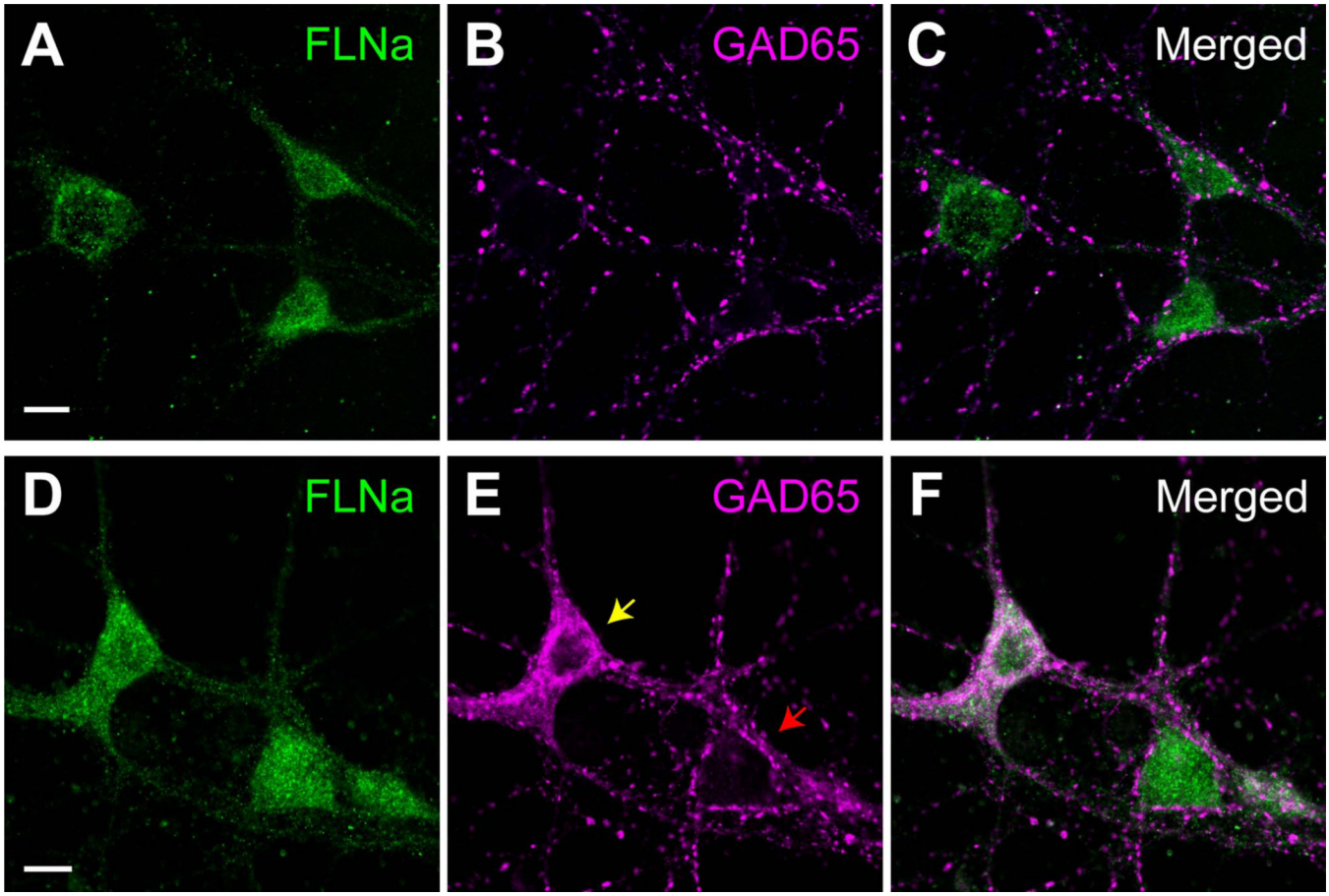


**Figure 10.**

FLNa immunoreactivity in principal and interneuronal populations. **A–C:** FLNa immunoreactivity in principal neurons is demonstrated by colabeling of primary hippocampal neurons (3–4 weeks *in vitro*) with FLNa and the interneuronal marker GAD65. Principal neurons, which do not express GAD (and form the majority of cells in culture), are typically characterized by the lack of somatic GAD signal. A network of punctate labeling surrounding the soma and dendrites represents presynaptic, inhibitory terminals. **D–F:** FLNa expression in interneurons, as demonstrated by the FLNa immunoreactivity of a GAD65-positive neuron (yellow arrow). The red arrow indicates a neighboring, GAD65-negative (presumably principal) neuron. Scale bars = 20 μm in A (applies to A–C); 20 μm in D (applies to D–F).

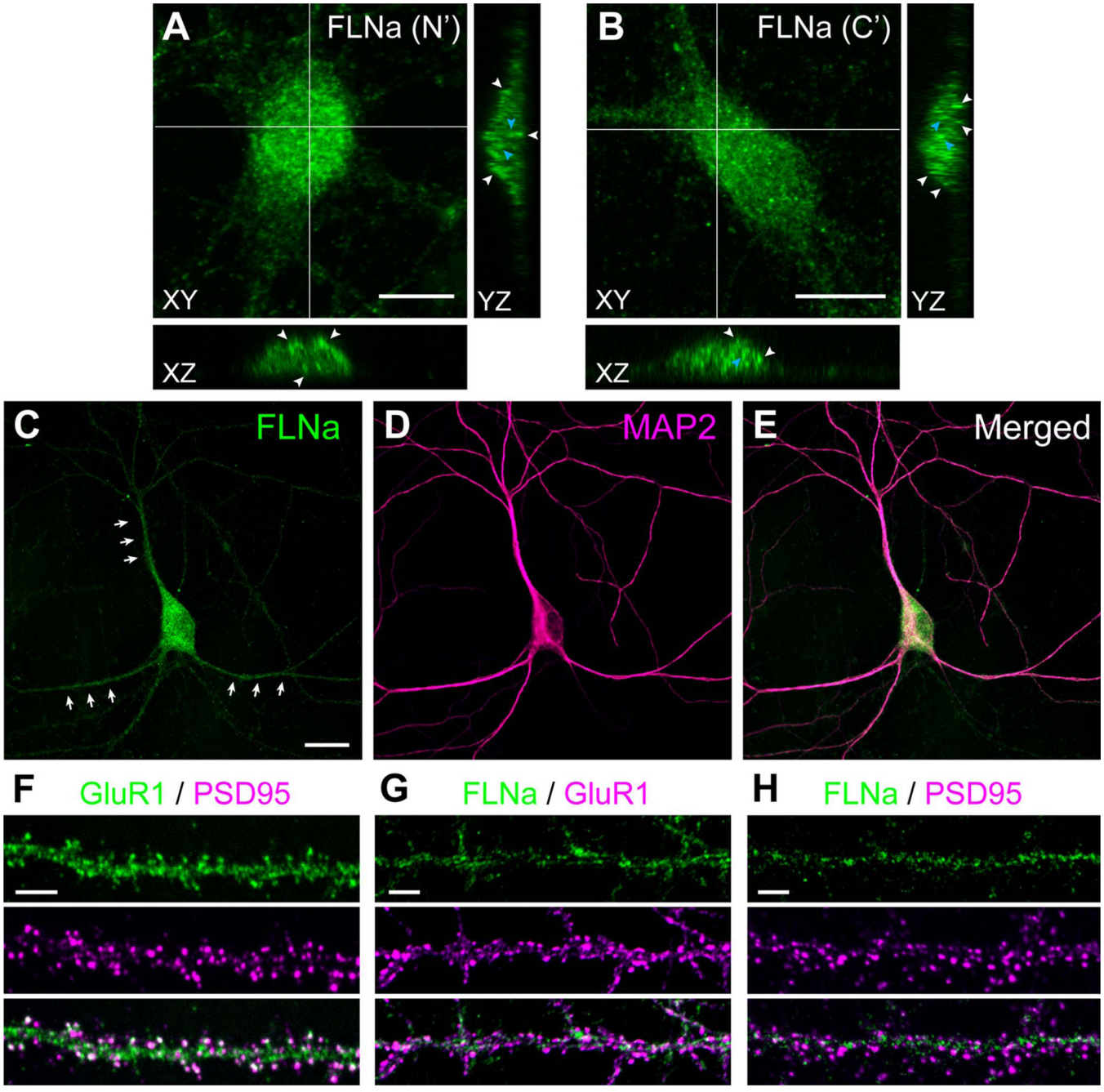


**Figure 11.**

Subcellular localization of FLNa. **A,B:** The distribution of FLNa signal in somata of primary hippocampal neurons, as demonstrated using FLNa antibodies directed against the N′ terminus (A) or the C′ terminus (B) of the protein. The images depict a confocal z-stack of optical slices at <1 μm thickness, with orthogonal views at the XZ and YZ axes. Puncta were found both within intracellular domains (light blue arrowheads) as well as near the surface of the cell lining (white arrowheads). **C–E:** FLNa-ir presence in dendrites, demonstrated by the colabeling of FLNa with the dendritic marker MAP2. **F–H:** Localization of FLNa to the dendritic shaft. Whereas spines are enriched in both GluR1 receptors and the postsynaptic protein PSD-95 (F), FLNa did not colocalize with either GluR1 (G) or PSD-95 (H) but

rather was detected as puncta along the shaft. Scale bars = 10 μm in A,B; 10 μm in C (applies to C–E); 5 μm in F–H.

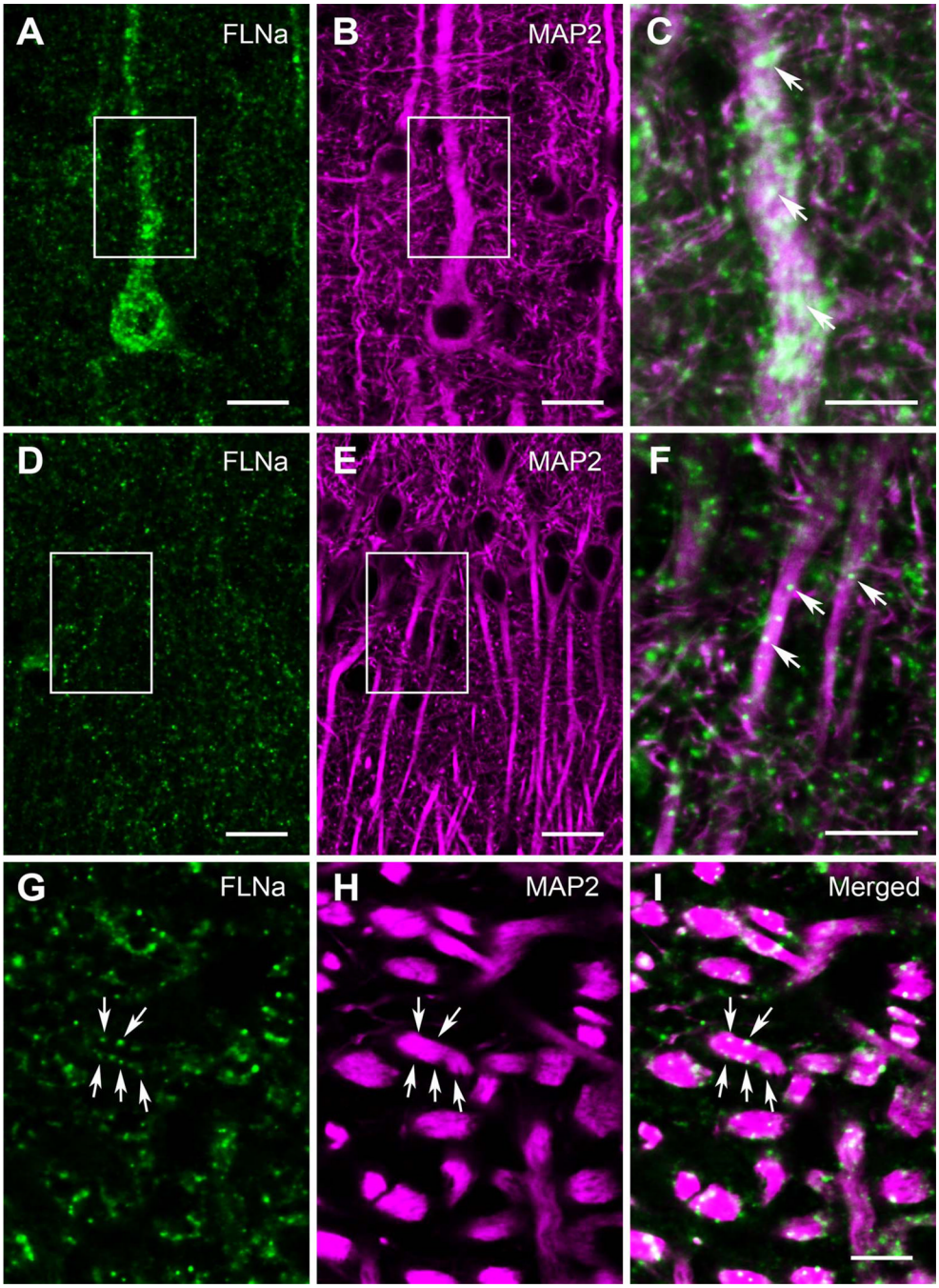


**Figure 12.**

Confocal images demonstrating the dendritic localization of FLNa immunoreactivity in the cortex (**A–C**) as well as in hippocampal CA1 (**D–F**) and CA3 (**G–I**) regions. In A–F, dual labeling of FLNa (green) and the dendritic marker microtubule-associated protein-2 (MAP2; magenta) revealed that most FLNa-ir puncta reside on the perimeter of dendrites of pyramidal neurons (arrows). FLNa was also rich in the somata of pyramidal neurons, possessing characteristics similar to those observed *in vitro* (Fig. 11). Boxed areas in A,B and D,E were merged and magnified in C,F, respectively. In the CA3 area (G–I), the primary dendrites of pyramidal neurons were cut off on the coronal section with a brush-like shape, revealing the perimembranous distribution of the FLNa-ir puncta (arrows). The

virtual slice thickness of all images is 0.5 μm. Scale bars = 20 μm in A,B,D,E; 10 μm in C,F; 10 μm in I (applies to G–I).

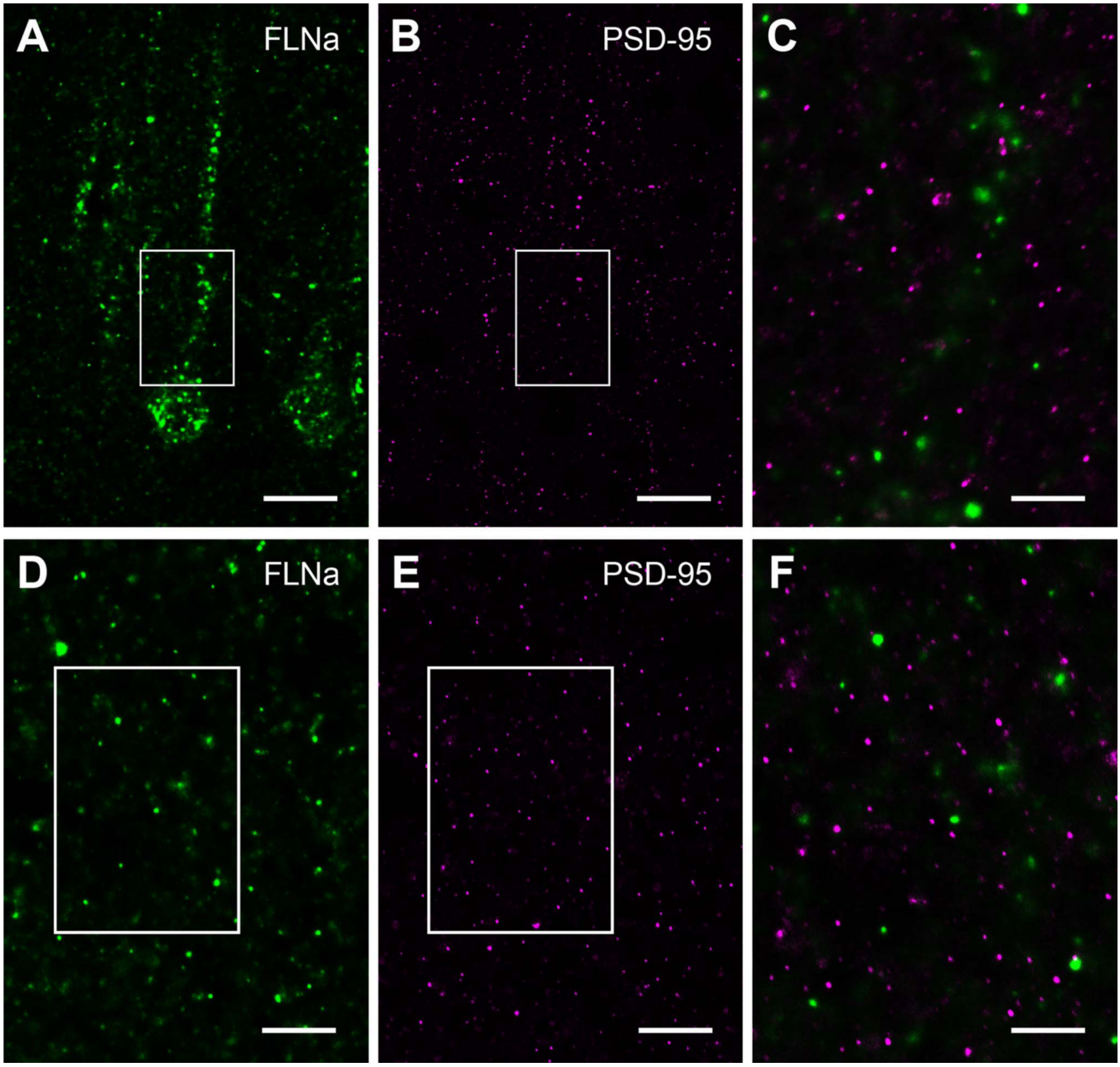


**Figure 13.**

FLNa-immunoreactive signal was not detected on the head of dendritic spines, indicated by the postsynaptic marker PSD-95. Dual labeling of FLNa (green) with PSD-95 (magenta) failed to demonstrate a postsynaptic location of FLNa-ir puncta in layer V of neocortex (**A–C**) as well as in the stratum radiatum of hippocampal CA1 (**D–F**). FLNa-ir puncta were frequently detected on the dendritic shaft (as also shown in Fig. 12) but not on the postsynaptic density. Boxed areas denote regions magnified in C,F. Optical slice thickness was 0.2 μm. Scale bars = 20 μm in A,B; 10 μm in D,E; 5 μm in C,F.

## TABLE 1

Primary Antisera Used in This Study

| Antiserum | Immunogen | Manufacturer, host, type | Dilution |
|---|---|---|---|
| Anti-FLNa | Purified human platelet membrane; recognizes full-length filamin and the N′ terminus 190-kDa calpain cleavage fragment of FLNa | Millipore (MAB1678), mouse monoclonal (clone PM6/317) | 1:1,000 WB<br>1:1,000 IF-C |
| Anti-FLNa | C′ terminus of recombinant human FLNa (aa 2348–2647), located at the C′ terminal 90-kDa calpain cleavage fragment | Santa-Cruz Biotechnology (H.300, sc-28284), rabbit polyclonal | 1:1,000 WB<br>1:1,000 IF-C<br>1:2,000 DAB<br>1:10,000 IF-TSA |
| Anti-actin | A synthetic peptide of 11 amino acids located on the C′ terminus of actin: SGPSIVHRKCF | Sigma-Aldrich (A2066), rabbit polyclonal | 1:100,000 WB |
| Anti-PSD 95 | Recombinant rat PSD-95 | Thermo Scientific (MA1-046), mouse monoclonal (clone 7E3-1B8) | 1:2,000 IF-C<br>1:2,000 IF-S |
| Anti-MAP2 | Purified rat brain microtubule associated protein; the antigenic site was identified as KNVRSKVGSTENIKHQPGGGRAK (Aizawa et al., 1989) | Sigma-Aldrich (M4403), mouse monoclonal (clone HM-2) | 1:25,000 IF-C<br>1:10,000 IF-S |
| Anti-GAD65 | Purified rat brain GAD; the antibody recognizes an epitope near the C′ terminus of GAD65 | Millipore (MAB351R), mouse monoclonal (clone GAD6) | 1:2,000 IF-C |
| Anti-GluR1 | Synthetic peptide corresponding to a sequence on human GluR1 C′ terminus (aa SHSSGMPLGATGL) | Millipore (AB1504), rabbit polyclonal | 1:1,000 IF-C |

IF-C, immunofluorescence, cultured neurons; IF-S, immunofluorescence, brain slices; IF-TSA, immunofluorescence, TSA amplification method; DAB, 3,3′-diaminobenzidine staining; WB, Western blot.

## TABLE 2

Distribution of FLNA-ir Neurons in the Rat Telencephalon: Density and Intensity

| Region | Density[1] | Intensity[2] |
|---|---|---|
| Olfactory bulb | | |
| Glomerular layer | + | +/++[3] |
| External plexiform layer | + | ++ |
| Mitral cell layer | ++++ | +++ |
| Internal plexiform layer | −/+ | + |
| Granular cell layer | −/+ | + |
| Accessory olfactory bulb | | |
| Mitral cell layer | ++++ | +++ |
| Granular cell layer | −/+ | + |
| Olfactory tubercle | | |
| Polymorphic layer | ++ | +/++ |
| Pyramidal layer | ++++ | ++ |
| Island of Calleja | ++ | +/++ |
| Taenia tecta | ++++ | ++ |
| Claustrum | ++++ | +/++ |
| Endopiriform nucleus | +++ | ++ |
| Neocortex | | |
| Layer I | −/+ | + |
| Layer II | ++++ | +++ |
| Layer III | ++++ | +/++ |
| Layer IV | ++++ | + |
| Layer V | ++++ | +++ |
| Layer VI | ++++ | +/++ |
| Frontal cortex | | |
| Layer II | ++++ | +++ |
| Layer IV | +++ | ++ |
| Layer V | +++ | +/++ |
| Entorhinal cortex | | |
| Layer II | ++++ | ++/+++ |
| Layer III–IV | +++ | ++ |
| Layers V–VI | +++ | ++/+++ |
| Perirhinal cortex | +++ | ++ |
| Hippocampal formation | | |
| Hippocampus | | |
| CA1 pyramidal layer | ++ | ++ |
| CA2 pyramidal layer | +++ | +++ |
| CA3a pyramidal layer | +++ | +++ |
| CA3b,c pyramidal layer | +++ | ++ |
| Dentate gyrus | | |

| Region | Density[1] | Intensity[2] |
|---|---|---|
| Hilus | ++ | ++ |
| Granular layer | +++ | + |
| Molecular layer | −/+ | + |
| Subiculum | ++ | + |
| Amygdala | | |
| Medial nucleus | ++ | + |
| Basomedial nucleus | ++ | + |
| Central nucleus | | |
| Medial | ++ | + |
| Lateral | ++ | +/++ |
| Basolateral nucleus | ++++ | +++ |
| Lateral nucleus | + | + |
| Bed nucleus of stria terminalis | | |
| Medial part | −/+ | + |
| Lateral part | −/+ | + |
| Basal ganglia | | |
| Caudate-putamen | − | − |
| Nucleus accumbens | + | + |
| Fundus striati | ++ | ++ |
| Globus pallidus | + | ++ |
| Ventral pallidus | ++ | +++ |
| Entopeduncular nucleus | ++ | +++ |
| Septum | | |
| Lateral septal nucleus | +++ | ++ |
| Medial septal nucleus | ++ | +/++ |
| Diagonal band of Broca | | |
| Vertical limb | +++ | +/++ |
| Horizontal limb | +++ | +/++ |

[1] Density values are based on the percentage of positive cells related to total cell number. −, No positive cells; −/+, occasional cells, <10%; +, low, 10–25%; ++, moderate, 25–50%; +++, dense, 50–75%; ++++, very dense, >75%.

[2] Staining intensity: +, weakly positive; ++, moderately positive; +++, intensely positive; ++++, strongly intense.

[3] Two scores are noted because the region contains cell populations with different labeling intensity.

## TABLE 3

Distribution of FLNA-ir Neurons in the Rat Diencephalon: Density and Intensity

| Region | Density[1] | Intensity[2] |
|---|---|---|
| Habenula | | |
| Medial part | +++ | +++ |
| Lateral part | + | + |
| Thalamus | | |
| Anterodorsal nucleus | ++ | ++ |
| Antroventral nucleus | ++ | ++ |
| Anteromedial nucleus | ++ | + |
| Mediodorsal nucleus | +++ | ++ |
| Lateral dorsal nucleus | + | + |
| Lateral postrior nucleus | ++ | ++ |
| Ventral lateral nucleus | +++ | ++ |
| Ventral postrolateral nucleus | ++ | ++ |
| Ventral postromedial nucleus | ++ | ++ |
| Paraventricular nucleus | + | ++ |
| Midline nuclear group | + | ++ |
| Intralaminar nuclear group | + | ++ |
| Thalamic reticular nucleus | + | + |
| Hypothalamus | | |
| Medial preoptic area | + | + |
| Lateral preoptic area | + | + |
| Suprachiasmatic nucleus | ++ | ++ |
| Retrochiasmatic nucleus | + | + |
| Supraoptic nucleus | ++ | ++ |
| Paraventricular nucleus | | |
| Medial parvocellular division | +++ | ++/+++[3] |
| Magnocellular division | −/+ | + |
| Ventromedial nucleus | +++ | ++/+++ |
| Arcuate nucleus | ++ | + |
| Anterior hypothlamic area | + | + |
| Lateral hypothalamic area | + | + |
| Dorsal hypothalamic area | +++ | ++ |
| Dorsomedial nucleus | +++ | +++ |
| Median eminence | −/+ | + |
| Subthalamic nucleus | ++ | + |
| Zona incerta | + | + |
| Medial geniculate body | + | ++ |
| Lateral geniculate body | + | ++ |

[1] Density values are based on the percentage of positive cells related to total cell number. −, No positive cells; −/+, occasional cells, <10%; +, low, 10–25%; ++, moderate, 25–50%; +++, dense, 50–75%; ++++, very dense, >75%.

[2] Staining intensity: +, weakly positive; ++, moderately positive; +++, intensely positive; ++++, strongly intense.

[3] Two scores are noted because the region contains cell populations with different labeling intensity.

## TABLE 4

Distribution of FLNA-ir Neurons in the Rat Hindbrain: Density and Intensity

| Region | Density[1] | Intensity[2] |
|---|---|---|
| Superior colliculus | + | + |
| Inferior colliculus | + | + |
| Tegmental nuclei | ++ | +/++[3] |
| Pedunculopontine nucleus | ++ | ++ |
| Red nucleus | ++ | +++ |
| Substantia nigra | | |
| Pars compacta | + | ++ |
| Pars reticulata | + | ++ |
| Raphe nuclei | | |
| Dorsal nucleus | +++ | ++ /+++ |
| Median nucleus | ++ | ++ |
| Edinger-Westphal nucleus | + | +/++ |
| Principal oculomotor nuclus | ++ | ++ |
| Darkschewitsch nucleus | ++ | ++ |
| Nuclei of the trigeminal nerve | | |
| Mesencephalic nucleus | ++++ | ++++ |
| Motor nucleus | ++++ | ++++ |
| Principal sensory nucleus | +++ | +++ |
| Spinal nucleus | ++ | +++ |
| Facial nucleus | ++ | +++ |
| Vestibular nuclei | + + | ++ |
| Cochlear nuclei | | |
| Dorsal nucleus | ++ | +/++ |
| Ventral nucleus | ++++ | ++ |
| Vagus nucleus | ++ | ++ |
| Hypoglossal nucleus | ++ | ++ |
| Solitary nucleus | ++ | +/++ |
| Locus coeruleus | + | + |
| Subcoeruleus | +++ | ++ |
| Superior olive | +++ | ++ |
| Inferior olive | +++ | ++ |
| Nuclei of lateral lemniscus | ++ | ++ |
| Nucleus of trapezoid body | | |
| Medial nucleus | ++++ | ++/+++ |
| Lateral nucleus | ++++ | ++/+++ |
| Cerebellum | | |
| Molecular layer | −/+ | + |
| Purkinje cell layer | ++++ | ++ |
| Granular cell layer | −/+ | + |

| Region | Density[1] | Intensity[2] |
|---|---|---|
| Cerebellar nuclei | + | + |

[1] Density values are based on the percentage of positive cells related to total cell number. −, No positive cells; −/+, occasional cells, <10%; +, low, 10–25%; ++, moderate, 25–50%; +++, dense, 50–75%; ++++, very dense, >75%.

[2] Staining intensity: +, weakly positive; ++, moderately positive; +++, intensely positive; ++++, strongly intense.

[3] Two scores are noted because the region contains cell populations with different labeling intensity.